Univerzita Karlova v Praze
Matematicko-fyzikální fakulta

DIPLOMOVÁ PRÁCE

Petra Matunová

Studium termodynamických a kinetických parametrů interakcí oligomerních modelů DNK s organokovovými komplexy aktivními v protirakovinné léčbě stanovených metodami kvantové chemie a kombinovanými QM/MM metodami

Katedra chemické fyziky a optiky

Vedoucí diplomové práce: prof. RNDr. Ing. Jaroslav Burda, DrSc.

Studijní program: Fyzika

Specializace: Biofyzika a chemická fyzika

Praha 2015

Charles University in Prague

Faculty of Mathematics and Physics

MASTER THESIS

Petra Matunová

Study of Thermodynamic and Kinetic Parameters for the Interactions of Oligomer Models of DNA with Organometallic Complexes Active in the Anticancer Treatment Determined by Quantum Chemical and Combined QM/MM Methods

Department of Chemical Physics and Optics

Supervisor of the master thesis: Prof. RNDr. Ing. Jaroslav Burda, DrSc.

Study programme: Physics

Specialization: Biophysics and Chemical Physics

Prague 2015

I would like to thank my supervisor Prof. Jaroslav Burda for his professional guidance during my work on the thesis. Also, I would like to thank my family for their support. As well, I would like to thank the Department of Chemical Physics and Optics and the employees of MetaCentrum organization for their computational resources.

I declare that I carried out this master thesis independently, and only with the cited sources, literature and other professional sources.

I understand that my work relates to the rights and obligations under the Act No. 121/2000 Coll., the Copyright Act, as amended, in particular the fact that the Charles University in Prague has the right to conclude a license agreement on the use of this work as a school work pursuant to Section 60 paragraph 1 of the Copyright Act.

In ..... date ..... signature of the author

Název práce: Studium termodynamických a kinetických parametrů interakcí oligomerních modelů DNK s organokovovými komplexy aktivními v protirakovinné léčbě stanovených metodami kvantové chemie a kombinovanými QM/MM metodami

Autor: Petra Matunová

Katedra: Katedra chemické fyziky a optiky

Vedoucí diplomové práce: prof. RNDr. Ing. Jaroslav Burda, DrSc., Katedra chemické fyziky a optiky, Matematicko-fyzikální fakulta, Praha

Abstrakt: Bylo prokázáno, že rutheniové a platinové komplexy jsou aktivní v protirakovinové léčbě. Dnes běžně používaná chemoterapeutika mají stále hodně negativních vedlejších účinků, proto je výzkum v této oblasti stále aktuální. První část diplomové práce se zabývá studiem cis-$[Pt(NH_3)_2Cl_2]$ (cisplatina, DDP) a čtyř platinových komplexů, potenciálních léčiv proti rakovině: $PtCl_2$(diaminocyklohexan), $PtCl_2(NH_3)$(cyklohexylamin) (JM118), cis-$[PtCl_2(NH_3)$(piperidin)] a trans-$[PtCl_2(NH_3)$(thiazol)]. Tyto komplexy jsou studovány v semi-hydratované a plně-hydratované formě. Termodynamické a kinetické parametry reakcí těchto komplexů s guaninem, což je klíčový proces pro zahájení protirakovinné aktivity, jsou studovány QM metodami. Analýzy elektronové hustoty byly provedeny na úrovni B3LYP/6-311++G(2df,2pd) v IEF-PCM modelu. V druhé části práce je studována reakce tzv. 'piano stool' komplexu ruthenia, $[Ru(II)(\eta^6$-p-cymen(nalidixová kyselina)(Cl)$]^+$, nejdříve s guaninem pomocí QM metod a poté s modelem ds-DNA pomocí QM/MM metod. Reakční centrum popisované QM metodami tvoří dva guaniny a Ru(II) komplex. Analýzy termodynamických a kinetických parametrů a analýzy elektronových hustot byly provedeny na úrovni B97D/6-31G*. Všechny studované reakce jsou exotermní a budou probíhat spontánně.

Klíčová slova: Termodynamické potenciály, chemická kinetika, organokovové komplexy, kvantová chemie

Title: Study of Thermodynamic and Kinetic Parameters for the Interactions of Oligomer Models of DNA with Organometallic Complexes Active in the Anticancer Treatment Determined by Quantum Chemical and Combined QM/MM Methods

Author: Petra Matunová

Department: Department of Chemical Physics and Optics

Supervisor: Prof. RNDr. Ing. Jaroslav Burda, DrSc., Department of Chemical Physics and Optics, Faculty of Mathematics and Physics, Prague

Abstract: It has been proven that platinum and ruthenium complexes are active in anticancer treatment. Nowadays, the common chemotherapeutica have a lot of side effects, therefore, drugs with fewer negative impacts are intensively searched for. The first part of the thesis focuses on the study of cis-$[Pt(NH_3)_2Cl_2]$ (cisplatin, DDP) and four platinum potential anticancer agents $PtCl_2$(diaminocyclohexane), $PtCl_2(NH_3)$(cyclohexylamine) (JM118), cis-$[PtCl_2(NH_3)$(piperidine)] and trans-$[PtCl_2(NH_3)$(thiazole)]. Thermodynamic and kinetic parameters of reactions of these complexes in semi-hydrated and fully-hydrated form with guanine were studied using QM methods. The reaction with guanine is the key process initiating the anticancer activity. Analyses of electron density were performed at the B3LYP/6-311++G(2df,2pd) level of theory in IEF-PCM model. The second part of the thesis studies the reaction of the so-called 'piano stool' Ru(II) transition metal complex, [Ru(II)(η^6-p-cymene(nalidixic acid)$(H_2O)]^{2+}$, first with guanine using QM methods and second with ds-DNA model using QM/MM methods. The reaction site, which is described by QM method, is two consecutive guanines and the Ru(II) complex. Analyses of thermodynamic and kinetic parameters, and electron density were performed at the B97D/6-31G* level of theory. All the mentioned reactions are exothermic and spontaneous.

Keywords: Thermodynamic potentials, chemical kinetics, organometallic complexes, quantum chemistry

Contents

Introduction **3**
0.1 Platinum complexes . . . 3
0.2 Ruthenium complexes . . . 5

1 Theory **9**
1.1 Quantum mechanics . . . 9
1.1.1 Atomic units . . . 9
1.1.2 Basic principles . . . 10
1.1.3 Born-Oppenheimer approximations . . . 11
1.1.4 Basis set . . . 11
1.1.5 Approximative methods in quantum chemistry . . . 12
1.1.6 Hartree-Fock method . . . 12
1.1.7 Density functional theory . . . 16
1.2 Effective core potentials . . . 18
1.3 Molecular mechanics . . . 19
1.3.1 Potential energy . . . 19
1.3.2 Force field . . . 22
1.3.3 Boundary conditions . . . 22
1.3.4 Geometry optimization algorithms . . . 24
1.4 Molecular dynamics . . . 24
1.4.1 Ergodic hypothesis . . . 25
1.4.2 Temperature and pressure evaluation . . . 25
1.5 Reaction thermodynamics . . . 27
1.5.1 Thermodynamics quantities . . . 27
1.5.2 Reaction kinetics . . . 28
1.6 Natural bond orbitals . . . 29
1.7 Hybrid QM/MM method . . . 30
1.7.1 Charge embedding . . . 32
1.7.2 Covalent embedding . . . 32

2 Methods **33**
2.1 Platinum complexes . . . 33
2.2 Binding of the Ru(II) complex to DNA . . . 35
2.2.1 QM calculations . . . 35
2.2.2 Molecular simulations . . . 37
2.2.3 ONIOM QM/MM simulations . . . 38

3 Results **42**
3.1 Platinum complexes . . . 42
3.1.1 Geometry parameters . . . 42
3.1.2 Energy profile . . . 47
3.1.3 Bonding and association energies . . . 52
3.1.4 Electron density analysis . . . 56
3.2 Reaction between the Ru(II) complex and guanine . . . 63
3.2.1 Geometry parameters . . . 65

3.2.2 Energy profile 66
3.2.3 Electron density analyses 67
3.3 Binding of the Ru(II) complex to DNA 69
3.3.1 Geometry parameters 71
3.3.2 Energy profile 73
3.3.3 Electron density analyses 76

Conclusion **79**

Bibliography **82**

List of Tables **86**

List of Abbreviations **88**

Introduction

Biochemistry and its principles have fascinated people for a long time. The biochemical systems represent rapidly developing areas in both experimental and theoretical levels. A huge expansion has occured in the computational chemistry field in recent decades. The current methods are quickly becoming more and more powerful and broader, allowing to study larger systems and to solve chemically related problems with higher accuracy.

However, the theoretical results must be compared with experiments in order to be able to judge, whether our results are meaningful. A vast number of different methods exists, which can be used for treating the investigated systems, but not all of the lead to reliable results.

Nowadays, with computational methods, we can obtain useful information about systems containing up to several hundred thousands of atoms depending on which approach is chosen.

Nucleic acids and proteins, key players in cells, are intensively studied currently. There is a lot of X-ray crystallography structures that commonly contain metal ions. Such metal ions usually have a significant influence on their biochemical and physical properties. Meanwhile, all biomolecules are composed of only few atoms (C, N, O, H, S, P), a lot of metal ions (Ca, Cu, Na, K, Mg, Fe, Zn, Co, ...) are often very specifically coordinated in biomacromolecules.

Pt and Ru transition metal complexes do not naturally occur in cells, however, due to their favorable properties, they are largely used for cancer treatment in pharmacology. Therefore, they can get inside the cells in the form of anticancer drugs.

0.1 Platinum complexes

The first discovered cytostatically active complex with antitumor effect was cisplatin, cis-$[Pt(NH_3)_2Cl_2]$ (DDP), Figure 1. It was discovered by chance in 1960's by Prof. Rosenberg, [1]. Since then, various organometallic complexes have been investigated in order to find a complex with better properties than cisplatin. Cisplatin is not applicable to all kinds of tumors and moreover, it has quite destructive side-effects such as hematopoiesis inhibition, hair loss, vomiting

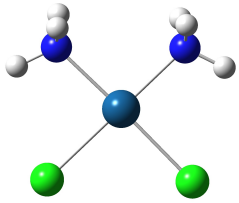

Figure 1: Cisplatin. Pt atom is in cyan, N atoms are in blue, Cl atoms are in violet and H atoms are in white.

or diarrhea, [2]. However, cisplatin is currently the most frequently used chemotherapeuticum, [3]. Discovery of a more specific anti-cancer drug would be a great step towards the cancer treatment.

The key feature when considering cisplatin is its interaction with DNA. The reaction pathway includes two reaction steps. First step is activation, where after the metallodrug penetrates into the cell, Cl^- ligand is released and replaced with a water molecule. The intracellular pH is lower than the extracellular pH. The environment inside the cells has a low concentration of chloride anions in contrast with the extracellular environment, which facilitates the hydration process. The resulting aqua-platinum complex is more reactive. Second step is the reaction of the aqua-complex with a nucleophillic centre that occurs in the cells (in proteins, nucleic acids), and the aqua-ligand of Pt is substituted by some nucleophille.

It is generally accepted that the interaction of transition metal complexes with a double-helix DNA is the key step for initiation of the anticancer activity of cisplatin. The preferred binding site is the N7 atom of guanine base, [4], Figure 2, which is located in the major groove of DNA.

With the highest probability, cisplatin creates an intra-strand bridge between two adjacent guanine bases. Such cisplatin bridge perturbs the local structure of DNA. When the cisplatin binding process is finished, the local structure of DNA is deformed and replication and transcription of DNA is blocked which may lead to apoptosis, a programmed death of the cell.

The first part of the thesis examines five Pt(II) complexes and aims to calculate interactions between them and guanine. These complexes are: the 'certified' drug cisplatin, as a benchmark, and

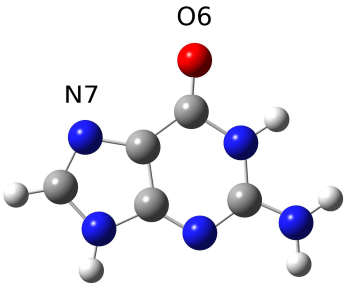

Figure 2: DNA base guanine. N atoms are in blue, O atom is in red, C atoms are in grey, H atoms are in white.

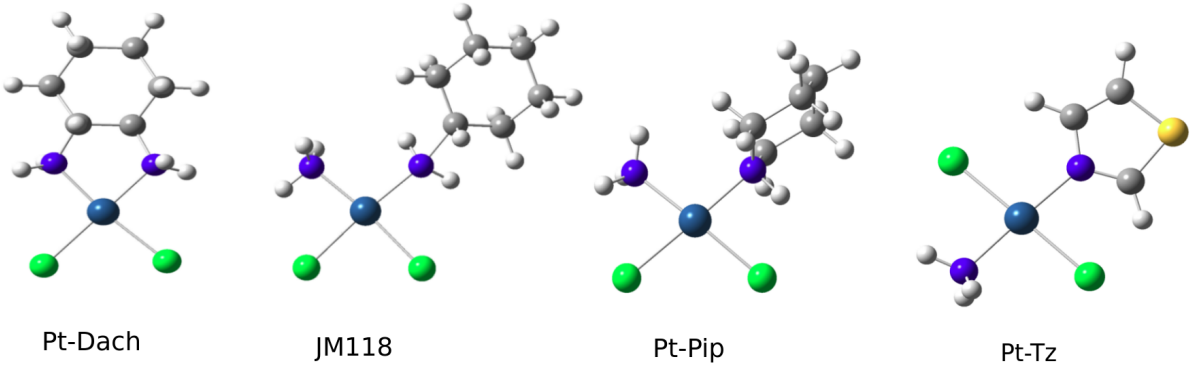

Figure 3: Platinum complexes: $PtCl_2$(diaminocyclohexane), $PtCl_2(NH_3)$(cyclohexylamine) (JM118), cis-[$PtCl_2(NH_3)$(piperidine)] and trans-[$PtCl_2(NH_3)$(thiazole)]. Pt atoms are in navy, N atoms are in blue, Cl atoms are in green, S atom is in yellow, C atoms are in grey and H atoms are in white.

four compounds with promising anticancer properties $PtCl_2$(diaminocyclohexane), $PtCl_2(NH_3)$(cyclohexylamine) (JM118), cis-[$PtCl_2(NH_3)$(piperidine)] and trans-[$PtCl_2(NH_3)$(thiazole)]. Their structures are shown in Figure 3.

The first reaction step, the hydration reaction, was studied in the literature [5]. Here, results from the second reaction step, where the water molecule is replaced by guanine, are presented.

0.2 Ruthenium complexes

The so-called 'piano-stool' ruthenium complex [Ru(II)(η^6-arene)(chelate)X]$^+$ is known for its cytostatic activity.

Arene is represented by benzene, p-cymene, biphenyl or dihydroanthracene; chelate is usually ethylenediamine (en) or acetylacetone (acac); X is Cl^-. The name 'piano-stool' describes the characteristic geometry of the Ru(II) complex, which resembles a piano stool.

The cytostatic activity of the Ru(II) complexes was discovered at the beginning of this century by Prof. Sadler in Edinburgh, who synthesized these complexes, [6]. Presently, their properties are intensively studied, both theoretically and experimentally. Such active complexes of transition metals may be used for chemotherapeutic treatment of tumour diseases in future. The 'piano-stool' ruthenium complexes are active against the cancer cells of line cisA2780, which are resistant to cisplatin.

For two Ru(III) complexes (NAMI-A and KP1019) was discovered very good anti-tumour activity. However, it is assumed that their oxidation state is reduced from +III to +II in biological environment. Therefore, the research has moved to Ru(II) complexes; as well, this thesis is focused on Ru(II) complex.

π-electrons of the arene cycle mediate the bond between the arene and the central Ru atom, which stabilize the Ru atom in its oxidation state. Also, the arene cycle ensures hydrofobicity of the whole complex, enabling to pass better through a cell membrane, [7].

Possible interactions between nucleic bases and the 'piano-stool' Ru(II) complexes of type $[Ru(II)(\eta^6\text{-arene})(en)Cl]^+$ has already been studied. Similarly, as in the case of Pt(II) complexes, two step reaction mechanism consisting of hydration and substitution reaction (involving the binding of the Ru(II) complex to guanine) was suggested also for the Ru(II) complex, [8]. Energetic profile for the activation reaction of [(benzene)RuII(en)Cl]+ complex and for following substitution reaction, where the aqua ligand is substituted with one of purine nucleic bases, was studied in ref. [9].

The preferred binding site for Ru(II) complex is again the N7 site of guanine, [6]. However, the reaction can proceed employing two reaction pathways. Either direct binding to the N7 atom or indirect binding with one intermediate state, where the Ru(II) complex is bound to the O6 atom of guanine.

Considering the change of the coordination of p-cymene ligand from η^6 to η^2-coordination, we get two available valences on Ru cation that interact with nucleophile guanine atoms. The saturation of free valences is assumed by coordination of N7 and O6 guanine

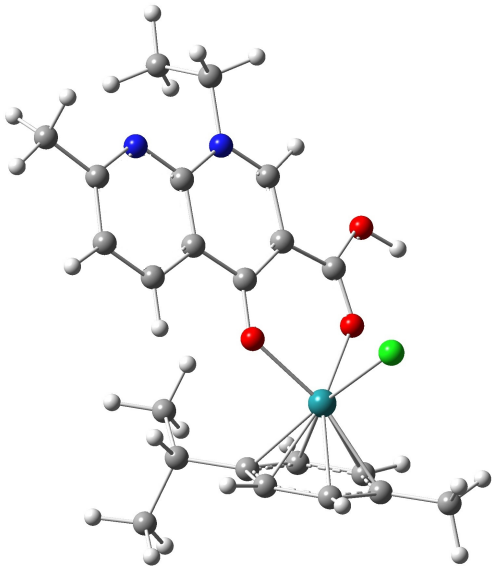

Figure 4: [Ru(II)(η^6-p-cymene(nalidixic acid)Cl]$^+$. Ru atom is in turquoise, Cl atom is in green, O atoms are in red, N atoms are in blue, C atoms are in grey, H atoms are in white.

atoms and water molecule. In final state, it is supposed that the p-cymene ligand is released from the Ru(II) complex.

From experimental measurements is known that the cytostatic activity of Ru(II) complexes is quite dependent on the size of the arene ligand and increases with its size. It is assumed that large arenes such as biphenyl or hydrogenated anthracenes can intercalate into DNA double-helix and deform its structure, [10].

The kind of chelate cycle and the concentration of chloride anions have influence on the speed and energetics of the reaction.

The second part of this thesis studies [(p-cymene)Ru(II)(nalidixic acid)Cl]$^+$ complex, Figure 4, and it aims to build realistic model of ds-DNA interacting with the Ru(II) complex. Computations of geometrical and energetic parameters of this models can explain the reaction mechanism of binding of the Ru(II) complex to DNA.

The description of the reaction mechanism of the 'piano-stool' Ru(II) complexes will be useful for practical usage of the Ru(II) complexes as well as for design of new Ru(II) complexes with anti-tumor properties. Generally, this work contribute to obtain better understanding of the behavior of transition metal complexes.

The detailed description of reaction mechanisms at the atomic level can be hardly obtained with experimental techniques. There-

fore, the computer simulations may improve our understanding of the anticancer effect of the Ru(II) complex.

In order to obtain realistic results using the computational molecular simulations methods, it is necessary to employ a more extended computational model involving the Ru(II) complex, oligomer model of ds-DNA and surrounding solvent. Major part of the work was carried out using QM/MM method combining quantum-mechanical description with molecular mechanics. This approach is suitable for exploration of chemical reactions of large bioorganical macromolecules like DNA.

1. Theory

1.1 Quantum mechanics

Quantum theory was developed at the beginning of the 20th century. It is adequate theory for proper description of molecules. To obtain properties, which depend on electronic structure of matter, for example charge transfer or bonding parameters, we need to use the quantum theory. The description using classical approach is usually not appropriate, especially if we would like to consider the formation and breaking of chemical bonds.

Although, quantum theory is in principle exact theory, in practical applications we need to employ certain approximations in quantum chemical protocols.

Quantum theory was summarized in many literature, for example [11], [12] and [13].

1.1.1 Atomic units

In quantum chemistry, the properties and quantities are described in atomic units, a.u., which are more suitable and reduce the number of constants in equations.

The unit of length is angström, 1 Å = 10^{-10} m, or Bohr radius, a_0,

$$a_0 = \frac{4\pi\varepsilon_0\hbar^2}{m_e e^2} \tag{1.1}$$

where ε_0 is the vacuum permittivity, m_e is the electron mass, e is the elementary charge and $\hbar$ is the reduced Planck constant. a_0 is equal to 0,052918 nm. It represents the most probable distance between electron and nucleus in hydrogen atom.

Commonly used energy unit is Hartree, Ha, which is equal to electrostatic potential energy of hydrogen atom. It is defined as follows:

$$E_a = \frac{\hbar^2}{m_e a_0^2} = \frac{m_e e^4}{16\pi^2\varepsilon_0^2\hbar^2} \tag{1.2}$$

In SI units, 1 Ha $= 4.3598 \cdot 10^{-18}$ J. Common energetic unit in thermochemistry is kilocalorie per mol, 1 kcal/mol = 4.184 kJ/mol; 1 Ha = 627.509 kcal/mol.

The atomic unit of mass is the weight of electron, $\mathrm{m}_e = 9,1095 \cdot 10^{-31}$ kg. The charge of electron represents the elementary charge, $e = 1.6022 \cdot 10^{-19}$ C.

The quantities in equations in following theoretical sections are presented in atomic units.

1.1.2 Basic principles

Quantum mechanics is based on a concept of wave function $\Psi(\mathbf{x}, t)$ that describes a state of given system. The wave function $\Psi(\mathbf{x}, t)$ can be obtained as a solution of Schrödinger equation.

The time dependent Schrödinger equation has the following form:

$$i\hbar\frac{d\Psi(\mathbf{x},t)}{dt} = \hat{H}(\mathbf{x},t)\Psi(\mathbf{x},t) \tag{1.3}$$

where $\hat{H}$ can be generally time dependent Hamiltonian of the system and $\hbar$ is reduced Plank's constant.

Its nonrelativistic and time independent form describing stationary states is defined as follows:

$$\hat{H}(\mathbf{x})\psi(\mathbf{x}) = E\psi(\mathbf{x}) \tag{1.4}$$

In the time independent case the wave function can be divided into time and spacial part, $\Psi(\mathbf{x}, t) = \psi(\mathbf{x})\varphi(t)$.

The Hamiltonian of a system is sum of quantum operators describing kinetic energy of nuclei, kinetic energy of electrons, electron-nuclei attraction, electron-electron repulsion and nucleus-nucleus repulsion:

$$\begin{aligned}\hat{H} = -\frac{1}{2}\sum_{A=1}^{N_n}\frac{1}{m_A}\Delta_A - \frac{1}{2}\sum_{i=1}^{N_e}\Delta_i - \sum_{i=1}^{N_e}\sum_{A=1}^{N_n}\frac{Z_A}{r_{iA}} + \sum_{i=1}^{N_e-1}\sum_{j=i+1}^{N_e}\frac{1}{r_{ij}} \\ + \sum_{A=1}^{N_n-1}\sum_{B=A+1}^{N_n}\frac{Z_A Z_B}{r_{AB}}\end{aligned} \tag{1.5}$$

where A and B index nuclei, i and j index electrons, N is number of respective particles, m and Z are their mass and charge.

1.1.3 Born-Oppenheimer approximations

Under certain assumptions, the wave function can be separated into a part depending on electron variables and into a part depending on nuclei variables. Considering the difference of at least three orders in the masses of electrons and nuclei, first, we can suppose that electrons move in an immobile field of nuclei due to their comparably negligible mass and high speed. Second, we can suppose that the nuclei move in effective field created by fast moving electrons.

In Born-Oppenheimer approximation, which solves the motion of electrons in the electrostatic field of fixed nuclei, the Hamiltonian has the following form:

$$\hat{H}_{BO} = -\frac{1}{2}\sum_{i=1}^{N_e}\Delta_i - \sum_{i=1}^{N_e}\sum_{A=1}^{N_n}\frac{Z_A}{r_{iA}} + \sum_{i=1}^{N_e-1}\sum_{j=i+1}^{N_e}\frac{1}{r_{ij}} + \sum_{A=1}^{N_n-1}\sum_{B=A+1}^{N_n}\frac{Z_A Z_B}{r_{AB}} \tag{1.6}$$

where the last term is an electrostatic interaction of nuclei, it is constant because of the assumed fixed nuclei. The time independent Schrödinger equation is solved without this term and the nuclei contribution to total energy is added afterwards.

1.1.4 Basis set

It is convenient to solve the time independent Schrödinger equation with the wave function $\psi(x)$ represented with a suitable set of basis functions. For example, with a set of atomic orbitals $\phi_i(\mathbf{x})$ which are practical for molecular systems. The wave function $\psi(x)$ is expanded into a Linear Combination of Atomic Orbitals, LCAO:

$$\psi(\mathbf{x}) = \sum_{i=1}^{K} c_i \phi_i(\mathbf{x}) \tag{1.7}$$

where c_i are expansion coefficients. The problem of solving Schrödinger equation is transformed into search for the c_i coefficients. The atomic orbitals $\phi_i(\mathbf{x})$ can be approximated by Slater type orbitals, STO, which are often expanded into series of Gaussian type orbitals, GTO, where atomic integrals are analytical.

1.1.5 Approximative methods in quantum chemistry

There are different variational and perturbation methods used in quantum chemistry when solving Schrödinger equation. They can be divided into three categories according to the level of the approximation. The most precise one are ab initio methods, where the Schrödinger equation is solved without any crucial approximation. Secondly, there are semiempirical methods, where the Schrödinger equation includes experimental parameters, the basis set has lower number of atomic orbitals and many electron integrals are neglected. And finally, very approximative empirical methods (e.g. Hückel method), where only the basic characteristics of molecules are taken into account.

1.1.6 Hartree-Fock method

The Hartree-Fock method is one-particle approximation to Schrödinger equation, where one electron is supposed to be in an effective field created by the other electrons. The antisymmetric condition to the wave function $\psi(\mathbf{x})$ is respected using Slater determinant:

$$\psi(\mathbf{x}) = \frac{1}{\sqrt{N_e!}} \sum_P (-1)^{sgn(P)} P[\chi_1(\mathbf{x}_1), ..., \chi_n(\mathbf{x}_n)] \tag{1.8}$$

where χ_j is a set of one-electron functions and P is permutation of electrons $\mathbf{x}_i$ and $sgn(P)$ is the signum function of P. The LCAO method is in this case applied on each molecular orbital instead of the total wave function.

Inserting the Slater determinant into the time independent Schrödinger equation and after applying variational principle, we get the Hartree-Fock equations:

$$[\hat{H}_1^{core} + \sum_{j=1}^{N_e} \hat{J}_j - \hat{K}_j]\chi_i(\mathbf{x}_1) = \varepsilon_i \chi_i(\mathbf{x}_1) \tag{1.9}$$

where each index of each operator is related to the index of the electron on which the operator act, $\hat{H}_1^{core}$ is one-electron Hamiltonian, $\hat{J}_j$ and $\hat{K}_j$ are Coulombic and exchange operators and ε_i is one-electron energy. The expression in square brackets is called Fock operator.

The Coulombic and exchange operators are defined as follows:

$$\hat{J}_i = \int dx_2 \chi_i^*(\mathbf{x}_2) r_{12}^{-1} \chi_i(\mathbf{x}_2) \tag{1.10}$$

$$\hat{K}_i = \int dx_2 \chi_i^*(\mathbf{x}_2) r_{12}^{-1} P_{12} \chi_i(\mathbf{x}_2) \tag{1.11}$$

where P_{12} is permutation operator. Solution of the Hartree-Fock equations is a set of molecular orbitals $\chi(\mathbf{x})$ resulting in expression for total energy E:

$$E = \sum_i \varepsilon_i - \sum_{i<j} (J_{ij} - K_{ij}) \tag{1.12}$$

The sums run over all occupied orbitals.

It is possible to express the total energy E by establishing one-electron integral H_{ii}:

$$E = \frac{1}{2} \sum_{i=1} (\varepsilon_i + H_{ii}) \tag{1.13}$$

where the sum run over all occupied orbitals and $H_{ii} = \int \chi_i^*(\mathbf{x}_1) \hat{H}_1^{core} \chi_i(\mathbf{x}_1) d\mathbf{x}_1$.

The Hartree-Fock equations are nonlinear nonlocal integro-differential equations, usually solved iteratively or using numerical methods.

The disadvantage is that the one-determinant representation of the wave function does not include dynamical correlation, because each electron is considered only in average field of the rest of the electrons. We can define correlation energy, E_{corr}, as the difference between the energy in HF limit E_{HF} and the exact nonrelativistic energy, E_{exact}:

$$E_{corr} = E_{exact} - E_{HF} \tag{1.14}$$

Closed shells

For closed shell system, the total spin of the system is equal to zero and every one-electron level is occupied by two electrons with opposite spins. The spacial parts the of wave functions of both of the electrons at the same one-electron level are the same. In this case, the Hartree-Fock equations lead to Roothaan's equations that have following form:

$$\sum_{\nu}[H_{\mu\nu}^{core} + \sum_{\lambda}\sum_{\sigma} P_{\lambda\sigma}((\mu\nu|\lambda\sigma) - \frac{1}{2}(\mu\sigma|\lambda\nu))]c_{\nu i} = \varepsilon_i \sum_{\nu} S_{\mu\nu}c_{\nu i} \tag{1.15}$$

where $c_{\nu i}$ are expansion coefficients of molecular orbitals $\psi_i(\mathbf{r})$ that are defined as linear combination of atomic orbitals $\phi_\nu(\mathbf{r})$. $H_{\mu\nu}^{core}$ is one-electron integral. $(\mu\nu|\lambda\sigma)$ and $(\mu\sigma|\lambda\nu)$ are two electron Coulombic and exchange integrals, transformed into the set of atomic orbitals in chemical notation. $P_{\lambda\sigma}$ is density matrix,

$$P_{\lambda\sigma} = 2\sum_{i=1} c_{\sigma i}^{*} c_{\lambda i} \tag{1.16}$$

where the sum of expansion coefficients run over all occupied orbitals and $S_{\mu\nu}$ is overlap matrix.

The total energy has following form:

$$E = \frac{1}{2}\sum_{\mu}\sum_{\nu} P_{\nu\mu}(H_{\mu\nu}^{core} + F_{\mu\nu}) \tag{1.17}$$

where $F_{\mu\nu} = H_{\mu\nu}^{core} + \sum_{\lambda}\sum_{\sigma} P_{\lambda\sigma}[(\mu\nu|\sigma\lambda) - \frac{1}{2}(\mu\lambda|\sigma\nu)]$.

SCF method

The method employed for solving Hartree-Fock and Roothaan equations is called Self Consistent Field method, SCF. It is an iterative method because of the nonlinear character of the task. It includes following steps:

1. Calculation of matrix elements of $H_{\mu\nu}^{core}$, $S_{\mu\nu}$ and $(\mu\nu|\lambda\sigma)$.
2. Obtain a guess of the density matrix using computationally cheaper method.
3. Construct the Fock matrix.
4. Transformation of Fock matrix into a basis set where the overlap matrix $S_{\mu\nu}$ is identity matrix.
5. Solving the eigenvalue problem and back transformation in order to obtain coefficients $c_{\mu i}$.
6. Construction of new density matrix $P_{\lambda\sigma}$.

7. Decision whether a convergence was reached, whether the new density matrix doesn't differ more from the old one according to a set criteria. If the condition is not satisfied, return to the step number 3 with the new density matrix.

8. If the procedure is converged, use the obtained solution to calculate required quantities.

Common criterion for establishing convergence in SCF method is to require convergence for elements of the density matrix by demanding the standard deviation of successive density matrix elements to be less than a small quantity δ.

Open shells

For open shell systems, two spin states of electron, marked as α and β, have to be distinguished. This leads to Pople-Nesbet equations for two sets of molecular orbitals:

$$\sum_{\nu}[H_{\mu\nu}^{core} + \sum_{\lambda}\sum_{\sigma} P_{\lambda\sigma}^{T}(\mu\nu|\lambda\sigma) - P_{\lambda\sigma}^{\kappa}(\mu\sigma|\lambda\nu)]c_{\nu i}^{\kappa} = \varepsilon_i^{\kappa}\sum_{\nu} S_{\mu\nu}c_{\nu i}^{\kappa} \tag{1.18}$$

where $\kappa = \alpha, \beta$, $P^T = P^\alpha + P^\beta$ is total density matrix and $P_{\lambda\sigma}^{\kappa}$ is κ-spin density matrix,

$$P_{\lambda\sigma}^{\kappa} = \sum_{i}^{occ} c_{\sigma i}^{\kappa *} c_{\lambda i}^{\kappa} \tag{1.19}$$

The total energy for open shell systems in Hartree-Fock approximation is expressed as follows:

$$E = \frac{1}{2}\sum_{\mu}\sum_{\nu}[P_{\nu\mu}^{T}H_{\mu\nu}^{core} + P_{\nu\mu}^{\alpha}F_{\mu\nu}^{\alpha} + P_{\nu\mu}^{\beta}F_{\mu\nu}^{\beta}] \tag{1.20}$$

where $F_{\mu\nu}^{\alpha} = H_{\mu\nu}^{core} + \sum_{\lambda}\sum_{\sigma} P_{\lambda\sigma}^{T}(\mu\nu|\sigma\lambda) - P_{\lambda\sigma}^{\alpha}(\mu\lambda|\sigma\nu)$ and $F_{\mu\nu}^{\beta} = H_{\mu\nu}^{core} + \sum_{\lambda}\sum_{\sigma} P_{\lambda\sigma}^{T}(\mu\nu|\sigma\lambda) - P_{\lambda\sigma}^{\beta}(\mu\lambda|\sigma\nu)$.

Beyond Hartree-Fock approximation

The electron correlation can be described when Slater determinants corresponding to electron excitations are included in the wave function. The electron correlation is not included in the Hartree-Fock

method, however, it is implemented, for example, in Configuration Interaction methods, CI. The more determinants are considered the more computationally demanding the calculation is.

Another approach to calculate correlation energy is Perturbation Theory, PT. Hartree-Fock energy corresponds to the energy obtained from the zero order of PT. Moller-Plesset, MPn, methods (of different orders n), which originates from perturbation theory are frequently used.

Another group of methods for the correlation energy calculations is based on Coupled Clusters method, CC, where higher number of Slater determinants of various electron excitations are considered.

1.1.7 Density functional theory

While the methods described in the previous chapter are based on the principle of many particle wave function, the Density Functional Theory, DFT, works with electron density matrix functional instead. Its computational costs are relatively low while preserving good quality in comparison with the already mentioned computational methods; the exchange and correlation functionals can be modelled well.

Hohenberg–Kohn theorems

The DFT is based on two Hohenberg-Kohn theorems. According to the first Hohenberg-Kohn theorem, the ground state density of a system determines its external potential.

Supposing the normalization of electron density $\rho(\mathbf{r})$ to number of electrons N:

$$\int \rho(\mathbf{r}) d\mathbf{r} = N \tag{1.21}$$

The Hamiltonian of the whole system determined by the density is as follows:

$$\hat{H} = -\frac{1}{2}\sum_{i=1}^{N_e} \Delta_i + \sum_{i=1}^{N_e} v(\mathbf{r}_i) + \sum_{i=1}^{N_e-1}\sum_{j=i+1}^{N_e} \frac{1}{r_{ij}} \equiv \hat{T} + \hat{V}_{ext} + \hat{V}_{ee} \tag{1.22}$$

where $\hat{T}$ is the kinetic energy, $\hat{V}_{ext}$ is the external potential and $\hat{V}_{ee}$ is the electron-electron repulsion.

The second Hohenberg-Kohn theorem states the relation between the exact energy of the ground state E_0 and energy determined by density $\rho(\mathbf{r})$:

$$E_0 \leq E[\rho(\mathbf{r})] \tag{1.23}$$

The wave function of non-degenerated ground state of many-electron system is unequivocal functional of one-electron density $\rho(\mathbf{r})$. However, the theorems give no information about the form of the functional.

Kohn–Sham method

The Kohn-Sham method was established in order to find the ground state electron density. It is based on treating non-interacting reference system of electrons representing the real system. Using the Hohenberg-Kohn theorems, there is a relationship between the density of the real and the reference system. Similarly, as in Hartree-Fock method, we can represent the densities by one-electron orbitals, which leads to canonical Kohn-Sham equations:

$$[-\frac{1}{2}\Delta + v_{eff}(\mathbf{r})]\psi_i(\mathbf{x}) = \varepsilon_i\psi_i(\mathbf{x}) \tag{1.24}$$

where $\psi_i(\mathbf{x})$ are one-electron functions from which is constructed the density $\rho(\mathbf{r})$:

$$\rho(\mathbf{r}) = \sum_{i=1}^{N_e} |\psi_i(\mathbf{x})|^2 \tag{1.25}$$

and $v_{eff}(\mathbf{r})$ is effective potential:

$$v_{eff}(\mathbf{r}) = v(\mathbf{r}) + \int \frac{\rho(\mathbf{r}')}{|\mathbf{r} - \mathbf{r}'|} d\mathbf{r}' + v_{xc}(\mathbf{r}) \tag{1.26}$$

In the latter equation, $v(\mathbf{r})$ is potential of nuclei and $v_{xc}(\mathbf{r})$ is exchange-correlation potential.

The resulting total energy of the system is:

$$E = \sum_{i=1}^{N_e} \varepsilon_i - \frac{1}{2}\int \frac{\rho(\mathbf{r})\rho(\mathbf{r}')}{|\mathbf{r} - \mathbf{r}'|} d\mathbf{r}d\mathbf{r}' + E_{xc}[\rho] - \int v_{xc}(\mathbf{r})\rho(\mathbf{r})d(\mathbf{r}) \tag{1.27}$$

The task in Kohn-Sham theory is to derive approximations to the exchange-correlation energy functional $E_{xc}[\rho]$, while the kinetic energy, calculated under the assumption of non-interacting electrons, is almost correct.

The exchange-correlation energy E_{xc} can be separated into exchange, E_x, and correlation, E_c, part:

$$E_xc[\rho] = E_x[\rho] + E_c[\rho] \tag{1.28}$$

The exchange energy can be expressed using Local Density Approximation, LDA, assuming that locally, the density can be treated as a uniform electron gas:

$$E_x^{LDA}[\rho] = -\frac{3}{4}(\frac{3}{\pi})^{1/3} \int \rho^{4/3}(\mathbf{r})d(\mathbf{r}) \tag{1.29}$$

If the the Kohn-Sham orbitals were the same as the Hartree-Fock orbitals, the exchange energy would be the same as the energy computed by the Hartree-Fock method. Methods that include exact exchange are often denoted hybrid methods. For example, one of the most popular hybrid functional in calculations of organic molecules is B3LYP.

1.2 Effective core potentials

The methods described above neglect relativistic effects. Therefore, generally, they are suitable for atoms with atomic number less than 26 corresponding to Fe atom. Usually, for other atoms starting from Fe, relativistic effects are non-negligible. In order to avoid the relativistic description are reduce the number of electrons, the core electrons are modeled with a suitable function $\hat{W}$, so-called effective core potential (EPC). The Schrödinger equation is solved only for valence electrons.

For example, Stuttgart-Dresden pseudopotentials, $\hat{W}_{SD}$, has following form:

$$\hat{W}_{SD} = -\frac{Z-n}{r} + \sum_l \hat{W}_l(r)\hat{P}_l \tag{1.30}$$

where $\hat{W}_l$ is radial part of the pseudopotential and $\hat{P}_l$ is projection operator to angular momentum functions.

1.3 Molecular mechanics

For larger systems, generally having approximately more than hundreds of atoms, the quantum chemistry methods are not efficient instrument anymore. Therefore, molecular mechanics (MM) method based on classical mechanics is used. This approach is less computationally demanding, but it cannot describe effects connected with electronic structure, for instance, charges or creation and annihilation of a bond.

Molecular mechanics describes a potential function of a molecule by a series of charged solid balls connected by strings, corresponding to atoms and bonds between them. Although this approach is not exact, it is used for geometry optimization and monitoring changes of molecular systems with respect to time where quantum mechanics cannot be used due to the large size of the systems.

Molecular mechanics was summed up many times in literature, for example [14], [15] and [16].

1.3.1 Potential energy

The potential energy E in molecular mechanics is composed of two main terms:

$$E = E_B + E_{nB} \tag{1.31}$$

The first term E_B represents bonding interactions and second term E_{nB} stands for non-bonding interactions.

Bonding interaction

Bonding interaction E_B is composed of three terms:

$$E_B = E_b + E_{ang} + E_{tor} \tag{1.32}$$

The first term E_b is energy of bonds, the second term E_{ang} is bending energy and the third term E_{tor} is torsion energy.

The terms in bonding interaction are schematically shown in Figure 1.1.

The E_b term for bonding energy is created in order to be analytically expressed and continuously differentiable. It arises from Taylor expansion of potential energy in equilibrium geometry $\mathbf{r}_{eq}$.

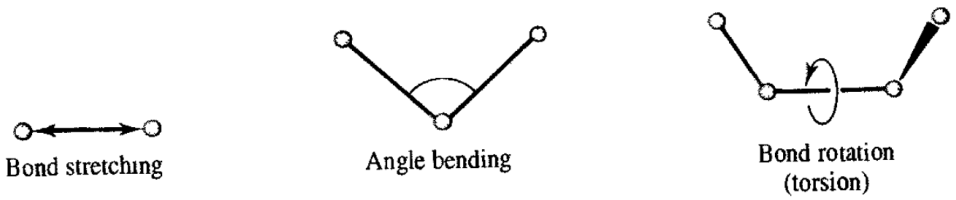

Figure 1.1: Bonding terms in molecular mechanics.

Usually, harmonic approximation is used where all the terms in the Taylor expansion higher than the second order are set to zero. The zero order term is constant. The first order term is zero due to the minimum condition on the potential energy surface. In the end, the only term left in the Taylor expansion is the second order contribution, a parabolic function.

The expression for the energy of bonds is a sum of contributions from all N_b bonds in the system:

$$E_b = \frac{1}{2}\sum_{i=1}^{N_b} k_i^b (r_i - r_{eq})^2 \tag{1.33}$$

where k_i^b is empirical constant which is included because of the unknown form of potential energy and its derivative.

The harmonic character of the function describes behavior of the system close to the equilibrium geometry well, but there is no proper description for long distances. Another option is Morse potential, E_b^M, which has the following form:

$$E_b^M = \sum_{i=1}^{N_b} D_i[1 - e^{-\alpha_i(\mathbf{r}-\mathbf{r}_{eq})}]^2 \tag{1.34}$$

where D_i is dissociation energy, a constant given either by experiment or computed with quantum chemistry methods, and α_i is another experimental fitting constant.

The bending energy E_{ang} is given by analogous expression:

$$E_{ang} = \frac{1}{2}\sum_{i=1}^{N_{ang}} k_i^{ang} (\varphi_i - \varphi_{eq})^2 \tag{1.35}$$

where φ_i is the angle between three bound atoms, N_{ang} is number of such angles and k_i^{ang} is force constant defining the shape of the

potential near the equilibrium value φ_{eq}.

Torsions have periodic character and they are described as follows:

$$E_{tor} = \frac{1}{2}\sum_{i=1}^{N_{tor}} k_i^{tor}[1 + cos(n\omega_i - \phi_{eq})] \tag{1.36}$$

where ω_i is torsional dihedral angle, ϕ_{eq} is phase shift, k_i^{tor} is force constant and n includes the periodicity of the system.

Non-bonding interactions

Non-bonding interactions E_{nB} are such interatomic interactions that are not mediated by chemical bonds. The E_{nB} is composed of two contributions, Coulomb energy E_{Coul} and Van der Waals energy E_{VdW}:

$$E_{nB} = E_{Coul} + E_{VdW} \tag{1.37}$$

The long-range Coulombic interaction is expressed as follows:

$$E_{Coul} = \frac{1}{4\pi\epsilon_0}\sum_{i=1}^{N-1}\sum_{j=i+1}^{N}\frac{Q_iQ_j}{r_{ij}} \tag{1.38}$$

where Q_i and Q_j are atomic charges.

The short-range Van der Waals interactions are frequently expressed with Leonard-Jones 12-6 function containing two empirical parameters, which differ for each type of atom. The first parameter, ϵ, stands for potential depth and the second parameter, r^0, is the interaction distance:

$$E_{VdW} = \sum_{i=1}^{N-1}\sum_{j=i+1}^{N}\epsilon_{ij}[(\frac{r_{ij}^0}{r_{ij}})^{12} - 2(\frac{r_{ij}^0}{r_{ij}})^6] \tag{1.39}$$

where $r_{ij}^0 = \frac{1}{2}(r_i + r_j)$ and $\epsilon_{ij} = \sqrt{\epsilon_i\epsilon_j}$.

The non-bonding interactions are computed separately for individual pairs of atoms. Due to the computational cost, the interactions are evaluated only up to a certain distance called cut-off. Elsewhere, they are set to zero.

1.3.2 Force field

Force field, FF, is a mathematical description of systems in molecular mechanics. It it a set of empirically gained or quantum-mechanically computed parameters.

Many general and specialized force fields were developed. The difference between various FF is in various terms that are included in the expression of total energy and interactions. Another difference is that different parameters are used. Different force field is the most convenient for every particular system, e.g. Universal Force Field, UFF, [17], for general-purpose usage. Another common force field is Assisted Model Building with Energy Refinement, AMBER, [24], used mainly for modeling of proteins and nucleic acids.

Beside other things, atom types for each atom are defined in force fields. The atom types consider even the neighboring atoms, therefore there are more atoms types than atoms.

For molecular mechanics calculations charges have to be specified, because they are crucial to the electrostatic forces. The charges are either obtained from the force field, computed quantum-mechanically or added by user.

1.3.3 Boundary conditions

For proper description of a system, the surrounding environment has to be included. If the system is periodic or if an infinite environment has to be considered, there arises question how to treat the boundary of the system. Common technique is to establish Periodic Boundary Conditions, PBC, which are based on replications of the system on the boundary. The principle of PBC is schematically shown in Figure 1.2.

Pair interaction in PBC method is computed in following way:

$$\mathbf{F}_{ij} = \sum_{n} \mathbf{F}(|\mathbf{r}_i - \mathbf{r}_j| + \sum_{\mu=1}^{3} a_\mu n_\mu) \tag{1.40}$$

where a_μ is the size of the box, μ determines the direction and $\mathbf{n}$ is a vector in the direction of the periodic images of basic cell.

Besides PBC, another approach is to include cut-offs. If there is a molecule on the boundary, there are several different possibilities.

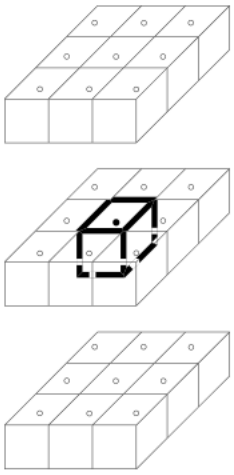

Figure 1.2: Schematic picture of a cubic simulation cell in the middle of another 26 periodic images emerging due to the PBC.

One is to use multipoles, where the system is divided into smaller cells and charges are computed as dipoles in the middle of each cell. Another possibility is to use non-bonding cut-offs. Here, the molecules that lie on both sides of the boundary are either whole figured in or, for instance, there is an interruption considering functional groups or atoms.

The cut-off can be applied together with a spline where the interruption is not sharp, but a suitable function ensuring continuous transition is applied.

Ewald summation

Frequently used method for treating the boundary of a system is Ewald summation. Within Ewald summation, every atom interacts with the rest of the atoms in a periodic image without the need to use cut-offs. This method is convenient for periodic systems. During computations, the calculations of non-bonding interactions are divided into direct and reciprocal space. The long-range contributions to total energy are evaluated in the reciprocal space. The precision of this method is relatively high, but it is more computationally demanding.

1.3.4 Geometry optimization algorithms

During geometry optimization we search for a structure corresponding to minimum of the multi-dimensional potential energy function. Such structure, a stationary state, is characterized by having all first derivatives zero and all second derivatives positive. Alternatively, stationary state can be a saddle point that has one negative derivative while the other are positive.

The most straightforward way is to step one variable (corresponding to one direction) at a time until the minimum is reached and then proceed with another variable. However, such approach is computationally very demanding. There are different methods commonly used for optimization, for example steepest descent or conjugate gradient method.

The steepest descent method can approach the minimum effectively, but it is not that convenient for obtaining the precise value of the minimum, it rather oscillates around it. Therefore, near minimum, this method it is often substituted with another one, which is more precise close to minimum. For example, the conjugate gradient method ensures far better convergence close to minimum.

1.4 Molecular dynamics

Molecular dynamics, MD, allows to investigate systems for a period of time, t. It is possible to investigate the time evolution of systems, and moreover, MD is frequently used for performing scan of the phase space in order to find a proper conformation of molecules or generate statistical ensembles. It is based on integrating the classical Newton's equations of motion, which describe the total force F_i acting on atom i that has the position $\mathbf{r}_i$:

$$F_i = -\frac{\partial V}{\partial \mathbf{r}_i} = m_i \frac{\partial^2 \mathbf{r}_i}{\partial t^2} \tag{1.41}$$

where V is potential of the system.

The coordinates can be obtained from the initial model of minimization, the velocities are generated randomly considering a given temperature.

Important parameter in molecular dynamic is time step. Too large time step can lead to instability and can cause inaccuracy. On

the other hand, too small time step takes too much computational time. The general limit for time step is restricted by the highest vibrational frequency. In organics it is the vibration of C-H bond, 10 fs. The time step is usually set between 0,5 and 1 fs.

Common method used for evaluating quantities with time in MD is Verlet method. It makes use of Taylor expansion of coordinates up to the second order forward and backward in time. As a result we get information about new position $\mathbf{r}(t + \delta t)$:

$$\mathbf{r}(t + \delta t) = 2\mathbf{r}(t) - \mathbf{r}(t - \delta t) + \mathbf{a}(t)\delta t^2 \tag{1.42}$$

where $\mathbf{a}$ is acceleration of the system. From here, explicit formula for velocities, velocity Verlet algorithm, can be derived.

The equation for the velocity $\mathbf{v}(t + \delta t)$ is as follows:

$$\mathbf{v}(t + \delta t) = \mathbf{v}(t) + \frac{1}{2}[\mathbf{a}(t + \delta t) + \mathbf{a}(t)]\delta t \tag{1.43}$$

1.4.1 Ergodic hypothesis

By including methods from statistical physics we can connect macroscopic parameters, like temperature or pressure, with the system that is described at the level of atoms. For general variable A its time average over molecular dynamics simulation, $\bar{A}$, can be stated. It is related to the statistical average by ergodic hypothesis:

$$\bar{A} \equiv \lim_{T\to\infty} \frac{1}{T} \int_0^T A(t)dt = \frac{\int\int A(\mathbf{r},\mathbf{p}) exp(-\frac{H(\mathbf{r},\mathbf{p})}{k_B T})}{\int\int exp(-\frac{H(\mathbf{r},\mathbf{p})}{k_B T})} d\mathbf{r}d\mathbf{p} \equiv \langle A \rangle \tag{1.44}$$

The limit is for practical purposes substituted with normalized sum over finite number of samples.

1.4.2 Temperature and pressure evaluation

Temperature and pressure are two important quantities that have to be considered during molecular dynamic simulation. Usually, they are kept fixed in order to ensure proper simulation conditions that demand chemical reactions. The temperature T is given by Boltzmann's equipartition theorem:

$$\frac{3}{2}Nk_BT = \langle \sum_{i=1}^{N} m_i v_i^2 \rangle \tag{1.45}$$

where N is the total number of particles in the ensemble and k_B is the Boltzmann's constant.

The pressure is controlled using virial theorem:

$$pV = Nk_BT - \frac{1}{3}\langle \sum_{i=1}^{N} \mathbf{r}_i \mathbf{F}_i \rangle \tag{1.46}$$

where V is the volume of the simulation box.

Thermostats

During MD simulations, the temperature is often kept fixed, particularly when canonical NVT ensemble is used. Various thermostat algorithms serve for these purposes, e.g. Andersen thermostat, Berendsen thermostat or velocity scaling.

Andersen thermostat algorithm is based on coupling the system with a fictitious heat bath bearing the demanded temperature. Stochastic impulsive forces ensure the coupling by acting randomly on particles of the investigated system. Frequency of the collisions represent the strength of the coupling. Temperature of such particles is reset according to the Maxwell-Boltzmann distribution for given temperature T:

$$P(v_i) = \sqrt{\frac{m}{2\pi k_B T}} exp(\frac{m v_i^2}{2k_B T}) \tag{1.47}$$

In Berendsen thermostat algorithm, the coupling with the bath is implemented by means of differential equation for temperature. It results in exponential decay of the former temperature with certain time constant. Velocity scaling algorithm controls temperature by scaling velocities with a factor depending on the fraction of the desired temperature and the real temperature.

For simulations with the NVT ensemble, the most fulfilling algorithm is the Andersen thermostat. Though the Berendsen thermostat acts better than velocity scaling algorithm from this point of view, it is still not completely satisfying.

1.5 Reaction thermodynamics

This part introduces thermodynamic quantities describing the course of chemical reactions in liquid environment. There is various literature concerning the reaction thermodynamics, for example [19] or [20].

For an ensemble of ideal gas made of noninteracting molecules and a low temperature, causing all the molecules to be in a ground state, the partition function, describing the entropy of the system, can be derived:

$$S = Nk_B + Nk_B \ln(\frac{q(V,T)}{N}) + Nk_BT(\frac{\partial \ln q(V,T)}{\partial T})_V \qquad (1.48)$$

where q is partition sum that contains contributions from rotational, vibrational, translation and electronic motion. The total partition function is obtained as a product of the mentioned contributions.

1.5.1 Thermodynamics quantities

Often, during calculations of chemical systems, the temperature T and pressure p are kept fixed. Therefore it is convenient to use Legendre transformation and derive Gibbs free energy, G, which is the thermodynamic potential that is minimized when the mentioned conditions are applied:

$$G = U + pV - TS \qquad (1.49)$$

where U is internal energy and S is entropy of the system.

The Gibbs free energy represents the reaction energy, it can be computed for two separate states of the system independently on the reaction pathway. For product P and reactant R we can state:

$$\Delta G = \sum_i G_i^P - \sum_i G_i^R \qquad (1.50)$$

This equation indicates whether the reaction is going to be spontaneous or not. The change in the Gibbs free energy between the transition state and the reactant represents the reaction barrier. Vibrational analysis of transition state is characterized by one imag-

inary frequency representing an antisymmetric movement between reactant and product state.

From quantum mechanical calculations it is possible to obtain corrections to total energy of computed system. For the contribution to the Gibbs free energy of reaction, G_{corr}, the following is valid:

$$G_{corr} = U + k_B T - TS \tag{1.51}$$

Due to the entropic term in the expression for the Gibbs free energy, it is computationally demanding to obtain the Gibbs free energy.

1.5.2 Reaction kinetics

Reactions in chemistry are processes happening until optimal concentration of reactants and products is reached. The suitable proportions are described with equilibrium constant, K:

$$K = \frac{[C]^c[D]^d}{[A]^a[B]^b} \tag{1.52}$$

Where the $[A]$ and $[B]$ are thermodynamic activities of reactants, $[C]$ and $[D]$ are thermodynamic activities of products and the powers are corresponding mols of their quantities.

Next, for the equilibrium constant, K, it is valid:

$$K = e^{-\Delta G/RT} \tag{1.53}$$

where ΔG is the Gibbs free energy difference between the product and the reactant of the reaction and R is the universal gas constant. We can see that for negative change of the Gibbs free energy ΔG the constant K is greater than 1 and therefore the concentration of products of the reaction increases and the reaction is spontaneous.

Rate constant, $k(T)$, quantifies the rate of the chemical reaction. In quantum-chemistry simulations, it is obtained using the Eyring transition state theory. The assumption is that the reaction proceeds along the reaction coordinate going through the lowest saddle point dividing the initial and final minimums on energetic hyperplain. The highest point on the reaction coordinate is called the transition state. The reaction rate is defined as follows:

$$k(T) = \frac{k_B T}{h} e^{-\frac{\Delta G^{\ddagger}}{RT}} \tag{1.54}$$

where h is Planck constant and $\Delta G^{\ddagger}$ is difference in the Gibbs free energy of the transition state and the reactant.

1.6 Natural bond orbitals

The solution to the electron Schrödinger equation are orbitals, which are delocalized. They do not correspond to the electron pairs localized on the corresponding nucleus or bond, as it would be correct from the chemical point of view. According to the Lewis theory, we want to find orbitals with the highest possible occupancy number corresponding to the electron pairs. Such orbitals are called natural orbitals, [21].

It is convenient to describe the distribution of electron density of a system with the wave function $\psi(1, 2, ..., N)$ using the first-order reduced density operator, $\gamma(1|1')$:

$$\gamma(1|1') = N \int \psi(1, 2, ..., N)\psi^*(1, 2, ..., N)d2...dN, \tag{1.55}$$

which is expanded in a basis set of atomic orbitals. The diagonal elements Γ_{ii} of the new density matrix $\boldsymbol{\Gamma}$ measure the occupancy of the corresponding atomic orbitals, which we want to maximize for occupied orbitals. After that we obtain different types of orbitals (natural atomic orbitals, NAO, natural hybrid orbitals, NHO, or natural bond orbitals, NBO), which differ in the space where the maximization is done.

If we maximize the occupancy for orbitals on atom A, partition the matrix $\boldsymbol{\Gamma}$ in atomic subblocks and consider the submatrix $\boldsymbol{\Gamma}_{AA}$ associated with the atomic orbitals on center A, then, after diagonalization of $\boldsymbol{\Gamma}_{AA}$ (with respect to the associated overlap matrix $\boldsymbol{S}_{AA}$), we obtain the natural atomic orbitals, n_A, as a linear combination of atomic orbitals localized at the corresponding atom:

$$\Gamma_{AA} n_i^A = p_i^A \boldsymbol{S}_{AA} n_i^A \tag{1.56}$$

Similarly, if we expand the space for maximization onto the space given by a basis on two atoms A and B, we obtain natural hybrid

orbitals. Before we proceed to diagonalization of the corresponding matrix $\boldsymbol{\Gamma}^{(AB)}$ (again with respect to the associated overlap matrix $\boldsymbol{S}^{(AB)}$), we subtract the density corresponding to the free electron pairs on atoms A and B, which are natural atomic orbitals n^A and n^B with occupancy numbers p^A close to two:

$$\boldsymbol{\Gamma'}^{(AB)} = \boldsymbol{\Gamma}^{(AB)} - \sum_{A,B} p_i^A n_i^A n_i^A \tag{1.57}$$

The obtained orbitals $h^{(AB)}$, which are doubly-occupied, can be decomposed into part h_A localized on atom A and into part h_B localized on atom B. The final hybrid orbitals are obtained from orthogonalization of corresponding orbitals n^A and h^A on the center A.

In the case of natural bond orbitals, we obtain, beside the one-center orbitals, also two-center orbitals. The one-electron reduced density is expressed in the NHO basis. From the diagonalization of the submatrices ${}^h\boldsymbol{\Gamma}^{(AB)}$ (with respect to the associated overlap matrix ${}^h\boldsymbol{S}^{(AB)}$) for all pairs of atoms A and B in this basis, we obtain the natural bond orbitals:

$$\Omega_{AB} = c_A h_A + c_B h_B \tag{1.58}$$

The c_A and c_B are polarization coefficients meeting normalization condition $c_A^2 + c_B^2 = 1$. Depending on the values of these coefficients, a bond NBO may range between covalent ($c_A = c_B$) and ionic ($c_A >> c_B$) limits.

Partial atomic charges, labeled as natural atomic charges Q_A, are obtained as a difference of proton number Z_A and a trace of diagonal block of reduced density matrix Γ_{AA} corresponding to the center A:

$$Q_A = Z_A - Tr\Gamma_{AA} \tag{1.59}$$

1.7 Hybrid QM/MM method

QM/MM method improve the classical approximation by combining the classical and the quantum approach, [16]. Usually, the important part of the system is treated quantum-mechanically, where the electron structure of the investigated system is considered, and

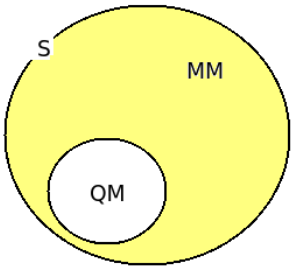

Figure 1.3: Schematic picture of system S composed of inner QM and outer MM part.

the rest of the system is simulated classically. The important part is usually the reaction center, where the important changes occur. Often it is only a small part of the whole system.

The complete Hamiltonian of the QM/MM system, Figure 1.3, is constructed from Hamiltonian containing the total interaction energy of the whole system computed with MM method, H_{Low}^{MM} , from Hamiltonian containing the total interaction energy of the QM part computed with QM method, H_{High}^{QM}, and from Hamiltonian containing the total interaction energy of the QM part computed with MM method, H_{High}^{MM}:

$$H_{complete} = H_{Low}^{MM} + H_{High}^{QM} - H_{High}^{MM} \tag{1.60}$$

If the boundary dividing the QM and MM part does not cross any chemical bond, the coupling between the two regions represented by $H_{QM/MM}$ can be computed in a relatively simple way. Considering a reaction in solution, the reaction system can be represented classically, and then energies and partial atomic charges computed in gas phase using QM methods are added.

Another solution, when the boundary does not cross any chemical bond, is to use more tightly coupled algorithms. Furthermore, it can be assumed that terms in $H_{QM/MM}$ take into account only non-bonded interactions. According to the desired level of precision, the interactions are considered as unpolarized, with polarized QM and unpolarized MM, or fully polarized.

1.7.1 Charge embedding

Van der Waals non-bonding interactions are obtained from the force field. There are various methods for obtaining the Coulombic interaction. Mechanical, electronic or polarized embedding can be employed.

In the case of mechanical embedding, the energy E_{ME} resulting from the electrostatic interaction is computed using the classical mechanics:

$$E_{ME} = \sum_{i=1}^{N_{MM}} \sum_{j=1}^{N_{QM}} \frac{q_i q_j}{r_{ij}} \tag{1.61}$$

where N is the number of corresponding particles and q stands for charges. The charges of the QM part have to be set in advance.

Electronic embedding is more precise method, where the QM electron density is polarized. The energy E_{EE} resulting from the electrostatic interaction is computed as follows:

$$E_{EE} = \sum_{i=1}^{N_{MM}} \int_V \frac{q_i \rho(\mathbf{r})}{|\mathbf{r}_i - \mathbf{r}|} d\mathbf{r} \tag{1.62}$$

1.7.2 Covalent embedding

If the QM/MM system contains a boundary passing through a covalent bond, joining the free valences between the two regions is a nontrivial problem. There are several ways how to treat the system, the QM bond has to be handled carefully.

One of the approaches is link atom method, where the cut bond is saturated with atom having one free valence. This link atom is then constrained to a line in order to get rid of the new related degrees of freedom. Then, the position of the atom is clear.

Disadvantage of this method is that the link atom is not usually chemically equivalent to the cut one. This can be solved, for example, with approach of frozen orbitals that belong to the cut MM part. Only orbitals involved directly in the former bond are free during the QM calculation.

2. Methods

Reaction mechanism of 5 different platinum derivatives mentioned in the introduction chapter interacting with guanine as well as the binding of the mentioned Ru(II) complex, [Ru(II)(η^6-p-cymene(nalidixic acid)(H_2O)]$^{2+}$, to DNA oligomer is studied using theoretical tools explained in the previous chapter.

The calculations were mostly carried out using clusters of Virtual Organization MetaCentrum, providing computational capacities. Also, computational clusters belonging to MFF UK were used, mostly for the analysis of the obtained results.

All static calculations were performed with the Gaussian 03, [22], or Gaussian 09, [23], computational chemistry program packages enabling to perform QM calculations.

Amber program was used for molecular dynamic simulations. Amber is a package of programs for molecular simulations, [24]. Its important part is called AmberTools, a set of independent programs that are able to cooperate with Amber. Besides other things, they serve the building of the simulated systems, their preparation for Amber simulations and also for structure, dynamic and energy-based analyses of trajectories obtained from MD simulations.

The visualizations of results were enabled by AIMStudio, [27], Molden, [28], VMD, [29], and GaussView, [30], software programs.

2.1 Platinum complexes

As it was explained in the introduction chapter, five Pt(II) complexes including cisplatin, $PtCl_2$(diaminocyclohexane), $PtCl_2(NH_3)$(cyclohexylamine) (JM118), cis-[$PtCl_2(NH_3)$(piperidine)] and trans-[$PtCl_2(NH_3)$(thiazole)] were calculated in their semi-hydrated and fully-hydrated form, after they were activated by hydration reaction.

The semi-hydrated complexes mean such complexes, where one of the Cl ligand of Pt is substituted with water. The fully-hydrated complexes mean such complexes, where one of the Cl atoms is substituted with water and the other one is substituted with OH^- group; in order to have the same total charge of both of the types of complexes, for the sake of comparison.

The Pt(II) complexes, one after another, are further in the thesis labeled as: DDP-Cl, Pt-Dach-Cl, JM118-Cl, Pt-Pip-Cl and Pt-Tz-Cl. The corresponding fully hydrated complexes are labeled with -OH endings.

Geometry of all structures: isolated reactants, reactant associates (both reactant molecules in supermolecular model), transition states, product associates and isolated products were optimized using the hybrid density functional B3LYP and 6-31+G(d) basis set. Explicit basis sets were used for the Pt, Cl and S atoms, the particular form can be found in attachment .1. The supermolecular model considers both interacting molecules as a single molecular H-bonded system. It allows to compare energies between structures within one reaction. The optimizations were performed first in vacuum and second, the surrounding environment was simulated using the IEF-PCM approach in order to describe solvent effects.

Different coordinations of guanine to the Pt(II) complexes in the reactant associates were optimized and the lowest energetic structure was chosen for further calculations. The same procedure was performed for water in the product associates.

Relativistic pseudopotentials from Stuttgart-Dresden laboratory were employed for the platinum core electrons (MWB-60) and for both second row elements, chloride and sulfur (MWB-10). The particular form can be found in attachment .2. The same computational level was used for the frequency analyses. The character of transition state was confirmed by a single negative eigenvalue of the hessian matrix that corresponds to the appropriate antisymmetric stretching mode.

Single point calculations were performed on optimized structures with the B3LYP functional and 6-311++G(2df,2pd) basis set. The original pseudoorbitals of Pt, Cl, and S were augmented by a set of appropriate diffuse and polarization functions, the particular form can be found in attachment .3. The NBO partial charges were used for rescaling the atomic radii of Cl, O, and S atoms in cavity construction in IEF-PCM model, [25], [26]. Furthermore, all the single point calculations were performed both with and without the BSSE corrections in the solvent environment as well as in vacuum.

Geometry parameters were evaluated on optimized structures.

Bonding and association energies (BE) of exchanging ligands for the stationary points on the reaction coordinate were computed

from the following equation: $BE = E_{complex} - E_L - E_{CL}$, where E_L is the BSSE corrected energy of the given ligand calculated with the ghost atomic orbital function on the complementary part of the whole structure and E_{CL} its complement calculated analogously. Also, the binding and association energies were computed for all the Pt ligands in isolated complexes.

NBO analysis of partial charges of Pt and its ligands was performed. NBO population analysis uses a set of atomic hybrid and bond orbitals; it corresponds well to the chemical intuition. It helps to understand the electron distribution within the system and also it clarify the geometrical changes during the reactions.

Bader's AIM analysis of electron density was employed for the evaluation of bond critical points of electron density (BCPs). BCP is a point between a pair of atoms, where the electron density has its minimum value. It describes binding interactions between pairs of atoms and their strength. Visualization program AimStudio was employed for the visualization of the BCPs.

Energetic quantities of the reactions of Pt complexes with guanine including reaction energies ΔE_r, Gibbs free energies of reaction ΔG, activation energy $\Delta E^{\ddagger}$ and Gibbs free energy of activation $\Delta G^{\ddagger}$ and their corresponding rate constants $k(298, 15)$ and $k_a(298, 15)$ of the reactions were computed using the refined energies from the single point calculations.

2.2 Binding of the Ru(II) complex to DNA

2.2.1 QM calculations

First, reaction between the Ru(II) complex, [Ru(II)(η^6-p-cymene(nalidixic acid)(H_2O)]$^{2+}$, and guanine is presented. The reaction was calculated using QM methods. The aim was to obtain a quick view into the reaction, which was after calculated in a larger model, as described in the sections below.

In the beginning, geometry of all structures: isolated reactants, reactant associates, transition states, product associates and isolated products were optimized using the DFT theory with the B97D Grimme's functional, [31], [32]. It is a functional from generalized gradient approximation class, GGA, approximating the exchange-

cor-
relation functional from the density and the actual coordinate. The B97D functional is an efficient and precise functional for large systems where it is important to include dispersion corrections. Based on previous studies, [9], this functional turned out to be suitable and with reasonable speed of calculation.

Optimizations of all stationary points were performed at three levels of theory. First, using less complex 3-21G* basis set and then employing more precise 6-31G* basis set. Last, the calculations were performed employing the 6-31G* and IEF-PCM approach for the description of solvent effects. The first number in the basis set specification indicates the number of primitive Gaussians that each core atomic orbital is comprised of. The second and third number indicates the number of primitive Gaussians that two basis functions, which create the valence orbitals, are comprised of, [33]. The * sign means that it contains d-polarization functions on heavy atoms.

For Ru, explicitly defined basis set was used. For 28 Ru core electrons, special explicit basis set together with relativistic pseudopotentials from Stuttgart-Dresden laboratory were used, the particular form can be found in attachment .6. For the optimizations using the 6-31G* basis set, the pseudopotentials on Ru were extended with one f and one g function. Also, for the Ru atom, an alternative radii of 1.75 Å for the use in fitting electrostatic potential-derived charges was set.

The same computational level was used for frequency analyses.

Different coordinations of guanine with respect to the Ru(II) complex in the reactant associates were optimized and the lowest energetic structure was chosen for further calculations. The same procedure was performed for water in the product associates.

Similarly, as in the case of the Pt(II) complexes, after the optimization calculations, single point calculations were performed on optimized structures with the B97D functional and 6-311++G(2df,2pd) basis set. The + sign stands for diffuse functions. The NBO partial charges were used for rescaling the atomic radii of O in cavity construction in IEF-PCM model.

Geometry parameters were evaluated on optimized structures. Gibbs free energies of the reaction of the Ru(II) complex with guanine were computed using the refined energies from the single point

calculations.

NBO analysis of partial charges of Ru and its ligands was performed. Bader's AIM analysis of electron density was employed for the evaluation of BCPs.

2.2.2 Molecular simulations

Larger computational model had to be taken into account when exploring binding to the oligomer model of DNA in comparison with the preceding calculations.

As explained in the introduction chapter, the Ru(II) complex, [Ru(II)(η^6-p-cymene(nalidixic acid)(H_2O)]$^{2+}$, the product of the preceding hydration reaction, was considered as reactant, labeled as R. In this part of the thesis, the binding process of the Ru(II) complex to DNA resulting in Ru(II)-N7 guanine monoadduct was explored.

Systems containing an oligomer model of B-DNA together with the investigated Ru(II) complex were built using the AmberTools programs. The oligomer model of B-DNA consists of 16 base pairs connected by sugar-phosphate bridges. Its sequence from the 5' to 3' end is following: GAA AAT GGC TAG CAG T; and the complementary part: CTT TTA CCG ATC GTC A. It contains two adjacent guanines in the middle, which is together with the Ru(II) complex the supposed reaction site. The Ru(II) complex approaches the DNA from the major groove.

Each of the build model was surrounded by about 6 thousand explicit waters using rectangular TIP3P water box. The structures were neutralized the with 28 Na^+ ions bearing positive charges. The oligomer model of B-DNA was negatively charged due to its negatively charged phosphate groups. The system was neutralized in order to simulate the real conditions well.

After the systems were build, minimization simulation proceeded using the conjugate gradients algorithm. The first 10 ps, the Ru(II) complex, DNA and the exchanging aqua-ligand of Ru were fixed and then for another 50 ps the minimization proceeded without any fixing. Consequently, temperature equilibration was done, the system was heated from 0 to 300 K during the time of 10 ps. Finally, pressure equilibration was done for 50 ps while keeping temperature on 300 K. The timestep during all the simulations was set to 1 fs.

For illustration of the MD simulations, the picture of the reactant

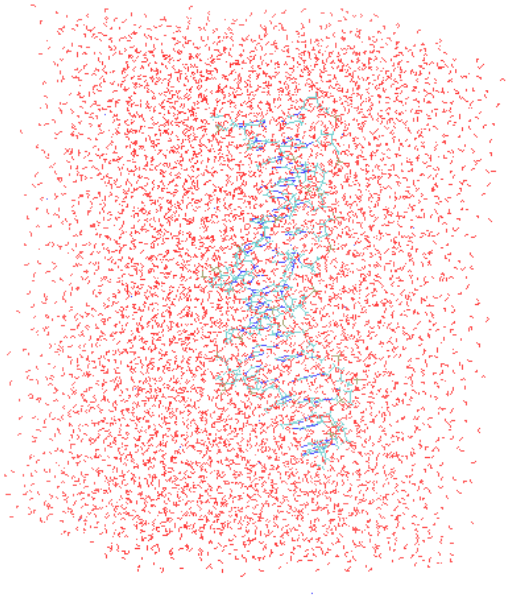

Figure 2.1: A snapshot from MD simulations containing the reactant of the binding process of the Ru(II) complex to DNA.

resulting from the MD simulations is shown in Figure 2.1. The picture of the reactant without the water box is shown in Figure 2.2.

2.2.3 ONIOM QM/MM simulations

The next step, after the MD calculations proceed, were QM/MM calculations. Gaussian 09 program with the ONIOM option, that enables the combination of QM and MM approaches, was employed for these calculations. The main purpose was to check the feasibility of the reaction and find stationary points on the reaction pathway in order to to get a proper view to the reaction and prepare structures which could be further inputted into more complex simulations enabling to perform MD sampling of the structures.

The Ru(II) complex together with the exchanging water, the oligomer of DNA and the Na^+ ions were extracted from the water box, which was used during the previous MD simulations. The Ru(II) complex together with the two guanines were the key part of the system and together with the exchanging water were described with a QM method. The QM/MM boundary of the system was crossing two glycosidic bonds between N9 atoms of both of the guanines and corresponding sugar bases. The link atom approach was

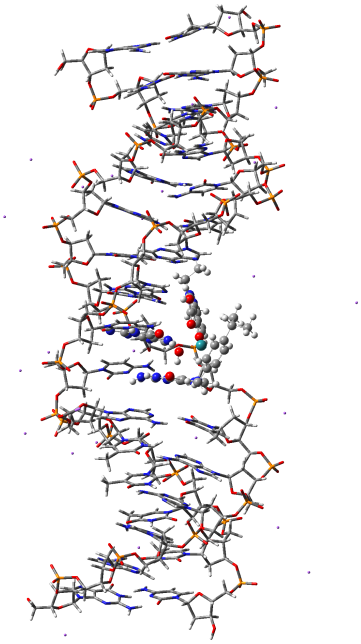

Figure 2.2: Reactant of the binding process of the Ru(II) complex to DNA resulting from MD simulations. The QM part of the system defined further is displayed in ball and bond type representation and the MM part is displayed in tube type representation.

used for the description of the boundary.

For the QM part of the system was used the DFT theory with the B97D functional.

Dispersion corrections using D2 version of Grimme's dispersion are included in B97D functional. Dispersion is an attractive Van der Waals type interaction between molecules as a result of instantaneous multipoles, especially in our case it describes stacking interactions between both guanines, so the realistic structure of DNA can be kept.

Optimizations of all stationary points were performed at two levels of theory. First, using less complex 3-21G* basis set and then employing more precise 6-31G* basis set. For Ru, explicitly defined basis set was used, the particular form can be found in attachment .2.

The same computational level was used for frequency analyses. The character of transitions states was confirmed by a single negative eigenvalue of the hessian matrix corresponding to the appropriate antisymmetric stretching mode. During transition states optimization, small optimization step of 0.01 Å was used.

The Ru atom was treated as in the case of the the QM calculations described above.

Density fitting approximation was used for the computation of the Coulomb interaction. Quadratically convergent procedure of 70 steps was called when the first-order SCF didn't converge. It comprises linear search when far from convergence and Newton-Raphson method when close to the convergence.

For the Ru(II) complex, two adjacent guanines and exchanging water was used the QM approach. Excluding the parts described with QM approach, the rest of the system including the remainder of the DNA (excluding the two QM guanines) together with the Na^+ ions was simulated with MM method, using AMBER force field which is suitable for biomolecules. Electronic embedding was employed to treat the interactions between QM and MM part.

The explicit waters were removed from the system and the ONIOM calculations were performed in vacuum. When trying to include water as an implicit solvent in Gaussian 09 program, the simulations were not running well. The jobs were computationally very demanding, considering the resources and the memory (at least 40 GB had to be specified for the calculation). It turned out that the Gaussian

09 program does not allow to perform the computations effectively in a reasonable time when the QM part is too big.

First, only the Ru(II) complex was optimized while keeping the rest frozen. Then, in next optimization, only the following parts were optimized: Ru(II) complex together with both of the guanines from the reaction center, their base pairs and three other closest base pairs above and below the reaction site.

Geometric parameters between Ru and its ligands were evaluated on optimized structures.

Further, electron density was analyzed on the QM part. First, using the NBO population analysis,[21], partial atomic charges of Ru atom and its ligands were evaluated. Second, Bader's AIM analysis of electron density was employed for the evaluation of bond critical points of electron density (BCPs). Visualization program AimStudio was employed for the visualization of the BCPs. All the analyses were performed at the level of theory described above.

3. Results

3.1 Platinum complexes

This section includes the results from the calculations of reactions of the Pt(II) complexes with guanine.

Schematic pictures of the reactants, transition states and products of the reactions of the semi-hydrated Pt(II) complexes with guanine are shown in pictures 3.1 - 3.5. The pictures of the fully-hydrated complexes are shown in attachment .4.

3.1.1 Geometry parameters

The Pt-ligand coordination bond lengths for the supermolecular structures of reactants, transition states and products of reactions of the Pt(II) complexes with guanine are included in Table 3.1. In Table 3.1, as well as in tables further in the text, label G stands for guanine and label Y stands for diaminocyclohexane, cyclohexylamine, piperidine or thiazole ligand of Pt.

Table 3.1 shows that the longest Pt-H_2O distance in reactants occurs in the Pt-Tz-Cl complex, about 0,03 Å more than in the rest of the cisplatin derivatives. The same is valid for guanine in products. The mentioned trend in the bond lengths can be caused by the trans influence effect; the Cl^- ligand has relatively large trans influence effect (enhances the substitution of the ligand trans to it) and increases the bond length trans to it. In the Pt(II) complexes with thiazole, in trans-position to the Cl^- ligand is water molecule and guanine, respectively, their corresponding bond lengths are the largest in this complexes in comparison with the rest of the Pt(II) complexes, where the water is in cis-position to the Cl^- ligand.

The analogous fact is valid for the OH^- ligand of Pt(II) as well. However, the Pt-OH distance and the distance between Pt and the trans-ligands of Pt are shorter than in the case of the Cl^- ligand; the Cl^- ligand has larger trans influence effect than the OH^- ligand.

In the case of DDP-Cl and DDP-OH, one of the amine group on Pt is in trans position to the Cl^- and OH^-, respectively. Considering the trans influence effect, we can distinguish these amino groups clearly.

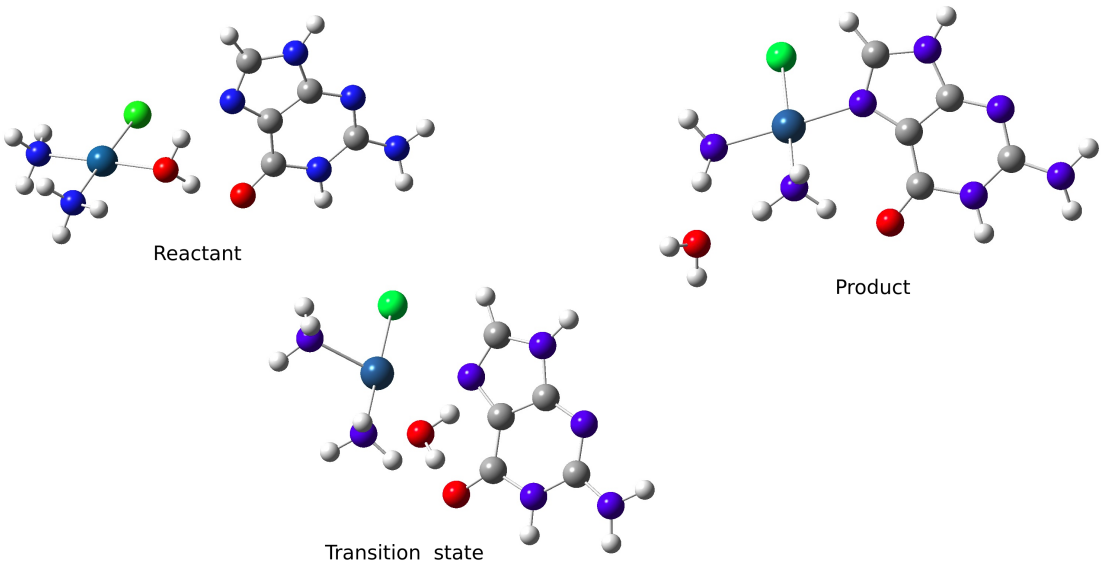

Figure 3.1: Reactant, transition state and product of reaction of DDP-Cl with guanine.

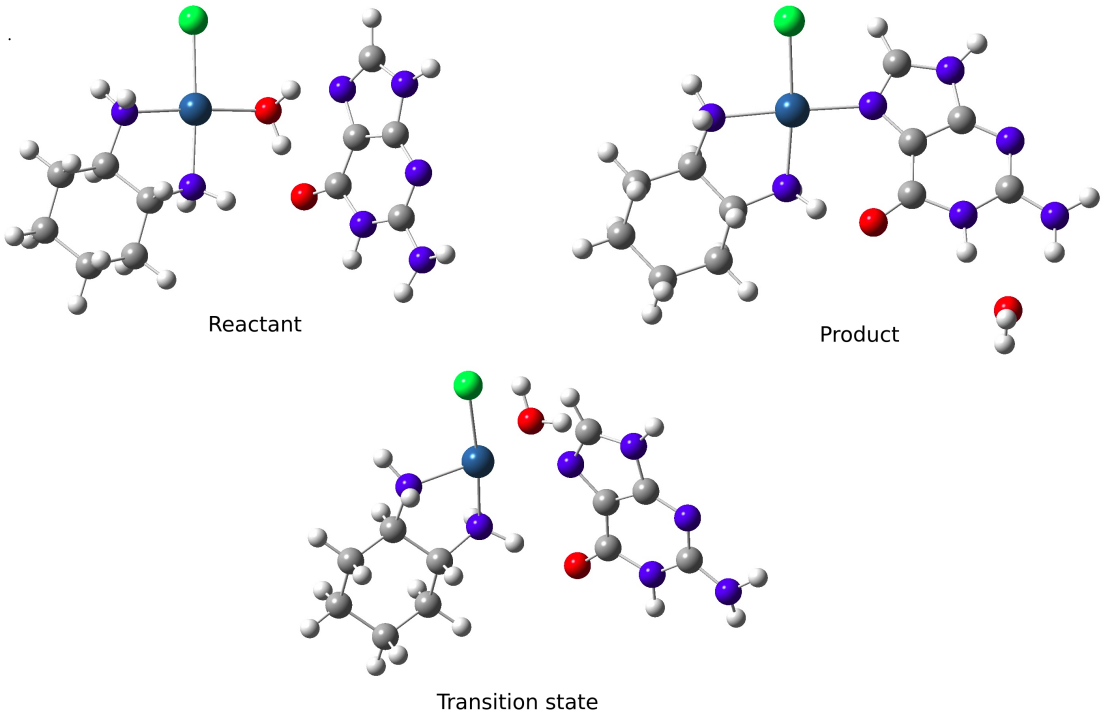

Figure 3.2: Reactant, transition state and product of reaction of Pt-Dach-Cl with guanine.

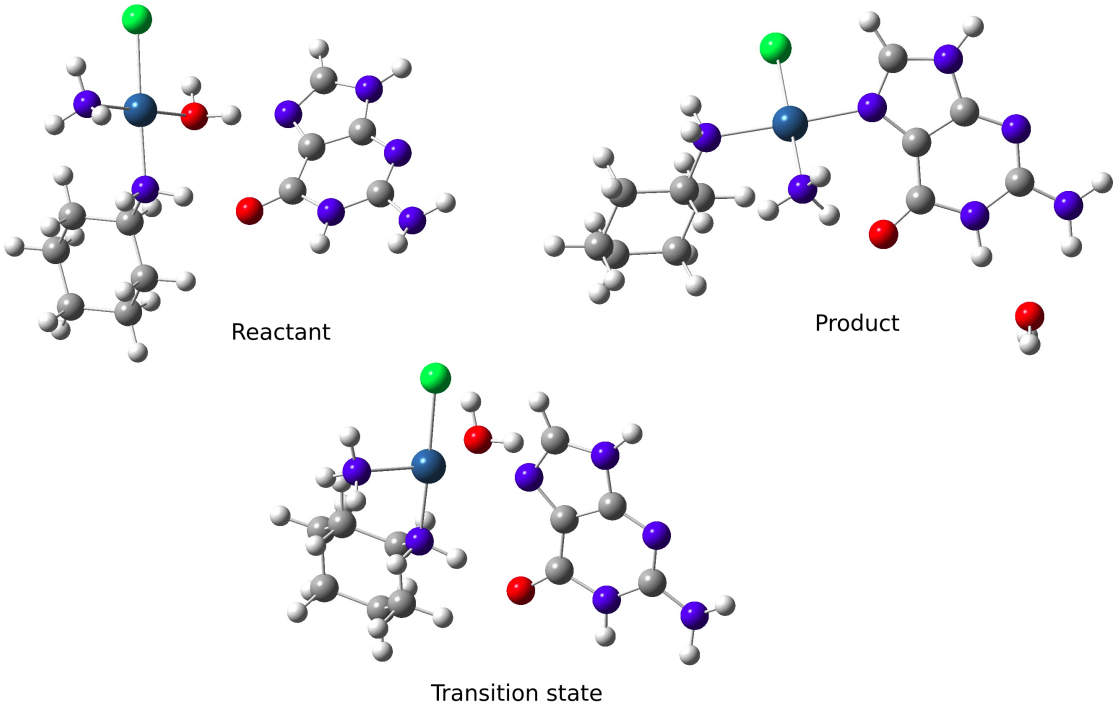

Figure 3.3: Reactant, transition state and product of reaction of JM118-Cl with guanine.

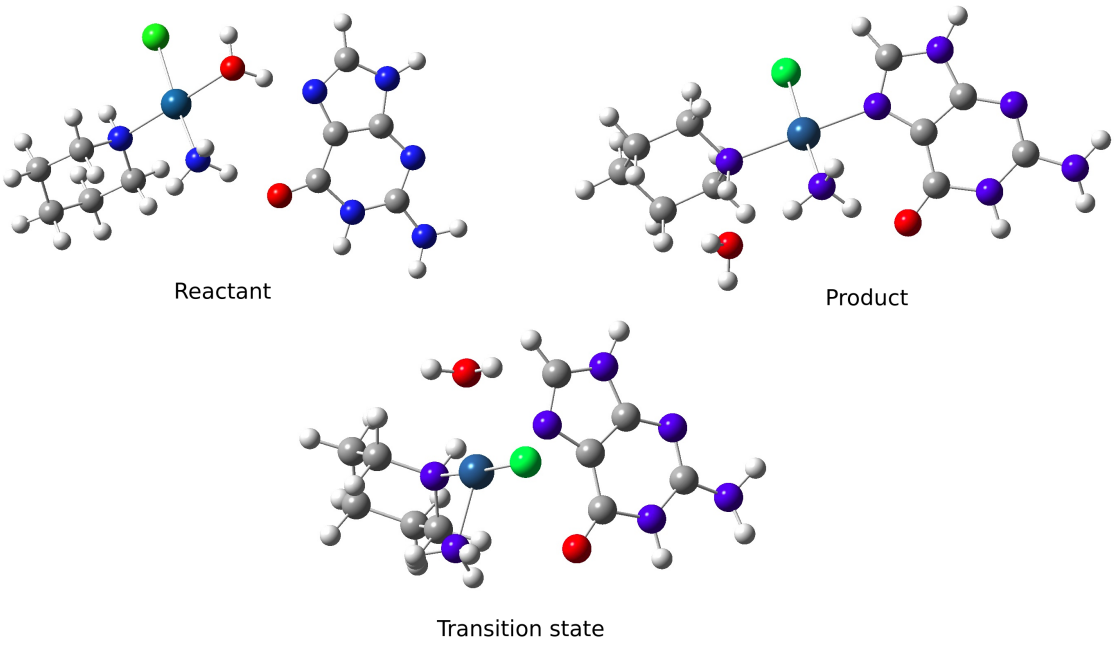

Figure 3.4: Reactant, transition state and product of reaction of Pt-Pip-Cl with guanine.

Table 3.1: The Pt-ligand bond lengths [Å] for the supermolecular structures of reactants, transition states and products of reactions of the Pt(II) complexes with guanine (B3LYP/6-31+G(d), IEF-PCM).

Complex	Cl /O(OH)	$O(H_2O)$	N7(G)	N(Y)	$N(NH_3)$
Reactants					
DDP-Cl	2,326	2,074	4,236	-	2,073[a]; 2,051[b]
DDP-OH	2,001	2,087	4,201	-	2,095[a]; 2,041[b]
Pt-Dach-Cl	2,371	2,094	4,064	2,075[a]; 2,046[b]	-
Pt-Dach-OH	2,004	2,096	4,126	2,098[a]; 2,041[b]	-
JM118-Cl	2,366	2,092	3,930	2,054	2,072
JM118-OH	2,009	2,088	4,069	2,058	2,092
Pt-Pip-Cl	2,370	2,094	3,991	2,063	2,072
Pt-Pip-OH	2,004	2,102	4,133	2,052	2,102
Pt-Tz-Cl	2,306	2,116	4,211	2,040	2,075
Pt-Tz-OH	1,973	2,132	4,215	2,032	2,073
Transition states					
DDP-Cl	2,365	2,449	2,541	-	2,074[a]; 2,055[b]
DDP-OH	2,001	2,482	2,569	-	2,098[a]; 2,041[b]
Pt-Dach-Cl	2,382	2,492	2,565	2,055[a]; 2,049[b]	-
Pt-Dach-OH	2,023	2,493	2,579	2,081[a]; 2,061[b]	-
JM118-Cl	2,384	2,514	2,572	2,072	2,052
JM118-OH	2,027	2,492	2,710	2,094	2,038
Pt-Pip-Cl	2,380	2,457	2,604	2,085	2,057
Pt-Pip-OH	2,027	2,496	2,634	2,103	2,053
Pt-Tz-Cl	2,361	2,420	2,575	2,040	2,066
Pt-Tz-OH	2,000	2,532	2,624	2,038	2,069
Products					
DDP-Cl	2,379	3,949	2,054	-	2,070[a]; 2,068[b]
DDP-OH	2,026	3,774	2,051	-	2,085[a]; 2,073[b]
Pt-Dach-Cl	2,382	7,262	2,058	2,067[a]; 2,069[b]	-
Pt-Dach-OH	2,026	3,504	2,050	2,067[a]; 2,082[b]	-
JM118-Cl	2,376	7,598	2,054	2,082	2,074
JM118-OH	2,023	3,709	2,056	2,081	2,085
Pt-Pip-Cl	2,384	4,006	2,062	2,090	2,074
Pt-Pip-OH	2,020	3,830	2,056	2,092	2,106
Pt-Tz-Cl	2,326	7,556	2,079	2,051	2,062
Pt-Tz-OH	1,987	7,674	2,089	2,062	2,058

[a] In trans-position to Cl^- or OH^- ligand of Pt

[b] In cis-position to Cl^- or OH^- ligand of Pt

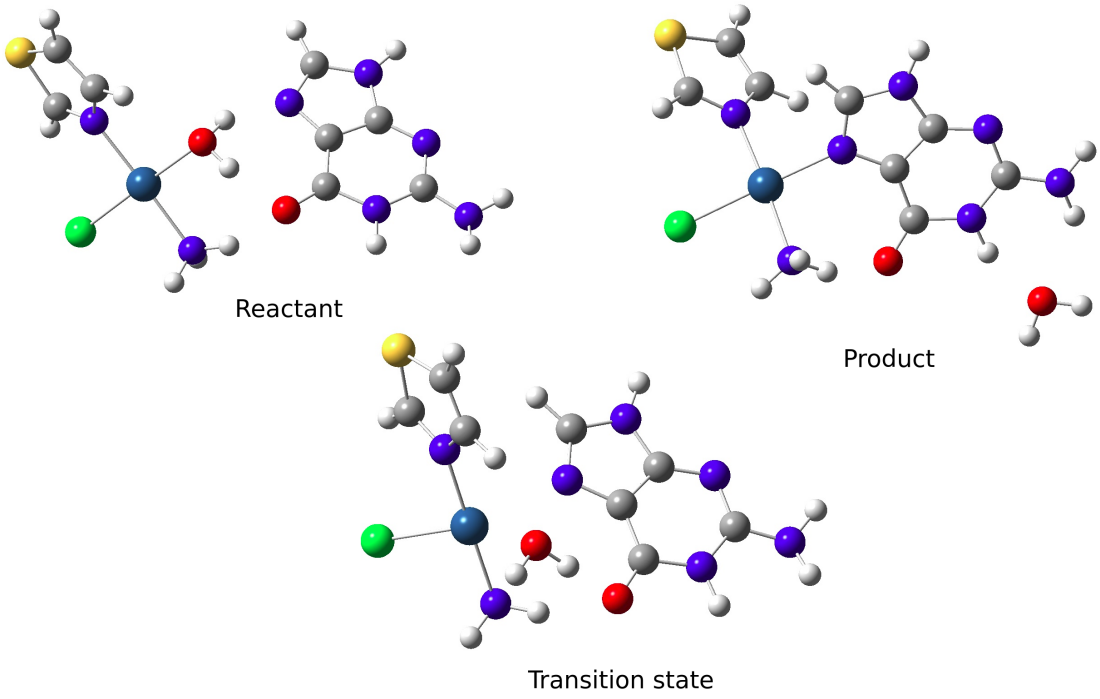

Figure 3.5: Reactant, transition state and product of reaction of Pt-Tz-Cl with guanine.

The bond lengths of the Y ligands in reactants are shorter than in products, the difference is about 0,03 Å. Generally, the bond lengths may be influenced by the steric effects, for example, stabilization of the structures with H-bonds. H-bonds occur mostly between O6 atom of guanine and an adjacent polarized H atom bound to N atom of one of the Pt ligands.

The shortest Pt-Cl distance occurs in the complexes with thiazole, about 0,05 Å less than in the rest of the cisplatin derivatives. The shortest Pt-N bonds are in the case of complexes containing thiazole, about 0,03 Å less than in the rest of the cisplatin derivatives. That is due to the π backdonation effect. The thiazole ligand is the only ligand that allows the π back donation from the Pt lone pair to the vacant orbital of N on thiazole.

The Pt-Cl bond lengths are longer than the Pt-OH bond lengths. The main reason is larger volume of Cl in comparison with O, therefore the distance to the Pt is increased.

The bond lengths corresponding to the OH^- ligands are about 0,1 Å shorter than the bond lengths corresponding to the H_2O ligands. That is due to the electrostatic interaction between the negatively charged OH^- ligand and the positively charged Pt.

In the transition states, the bond lengths between the exchanging water and the Pt are about 0,4 Å longer than in the reactants. The bond length between water and Pt in DDP-Cl complex is relatively long in comparison with the rest of the structures. That can be caused by hydrogen bonds between water and O6 of guanine, which is relatively strong nucleofilic centre. Similar effect can be seen in the case of Pt-Tz-Cl. For the rest of the structures, the O6 of guanine is not in close proximity to the water molecule.

The Pt-N7(G) it is about 0,05 Å shorter in products when comparing with Pt-O(H_2O) bond lengths in products. The bond lengths of the exchanging ligands in transition states could indicate that the ligand replacement passes through the associative mechanism. For the dissociative mechanism, the bond lengths would be increased.

3.1.2 Energy profile

Energetic quantities of the reactions of the Pt(II) complexes with guanine, including reaction energies ΔE_r, Gibbs free energies of reaction ΔG, activation energy $\Delta E^{\ddagger}$ and Gibbs free energy of activation $\Delta G^{\ddagger}$, both in IEF-PCM and in vacuum obtained from the single point calculations are presented in Table 3.2. The energies obtained from the optimization calculations are presented in Table 3.3. Their rate constants $k(298, 15)$ corresponding to the single point calculations are shown in Table 3.4. Gibbs free energy reaction profiles calculated in IEF-PCM are included in graphs in Figures 3.6 and 3.7.

Table 3.2 shows that all the reactions were exothermic and therefore spontaneous processes from the thermodynamical point of view. The preceding aquation processes were endothermic reactions, [5], which formed thermodynamically less stable systems, but occurred due to a low chloride concentration. The aqua-ligand was relatively unstable in the Pt(II) complexes.

Considering the energy values in the solvent model, the lowest Gibbs free energy of reaction was obtained for the Pt-Tz-Cl complex, ΔG = -5,5 kcal/mol. The highest Gibbs free energy of reaction was obtained for the Pt-Dach-Cl complex, ΔG = -13,3 kcal/mol. All the reaction barriers were lower in comparison with the DDP-OH complex, with the exception of the complexes containing piperidine, which was always significantly higher. The reaction barriers

Table 3.2: Thermodynamic quantities [kcal/mol] of stationary points of reactions of Pt(II) complexes with guanine resulting from 6-311++G(2df,2pd) single point calculations in IEF-PCM and in vacuum.

Complex	IEF-PCM [kcal/mol]				Vacuum [kcal/mol]			
	ΔE_r	ΔG	$\Delta E^{\ddagger}$	$\Delta G^{\ddagger}$	ΔE_r	ΔG	$\Delta E^{\ddagger}$	$\Delta G^{\ddagger}$
DDP-Cl	-8,9	-9,6	21,4	18,4	-12,9	-13,6	21,0	20,2
DDP-OH	-9,0	-8,9	22,0	21,8	-13,7	-14,8	20,4	20,0
Pt-Dach-Cl	-10,2	-13,3	18,3	21,3	-16,7	-16,8	15,8	16,3
Pt-Dach-OH	-13,6	-7,7	18,0	15,3	-10,6	-11,3	20,5	20,5
JM118-Cl	-10,4	-10,4	20,4	22,1	-12,4	-12,4	20,6	21,2
JM118-OH	-11,1	-10,4	23,5	17,4	-9,5	-11,7	22,8	22,2
Pt-Pip-Cl	-7,9	-6,8	27,0	29,9	-6,5	-6,8	28,4	28,8
Pt-Pip-OH	-8,8	-8,0	22,4	25,5	-3,3	-3,2	24,7	24,1
Pt-Tz-Cl	-5,3	-5,5	17,1	17,6	-6,1	-5,2	21,0	21,2
Pt-Tz-OH	-8,8	-10,0	17,7	21,1	-8,1	-7,1	21,6	21,9

Table 3.3: Thermodynamic quantities [kcal/mol] of stationary points of reactions of Pt(II) complexes with guanine resulting from 6-31+G(d) optimizations calculations in IEF-PCM and in vacuum.

Complex	IEF-PCM [kcal/mol]				Vacuum [kcal/mol]			
	ΔE_r	ΔG	$\Delta E^{\ddagger}$	$\Delta G^{\ddagger}$	ΔE_r	ΔG	$\Delta E^{\ddagger}$	$\Delta G^{\ddagger}$
DDP-Cl	-7,6	-9,0	20,7	20,5	-9,7	-9,0	20,6	21,5
DDP-OH	-10,9	-9,3	19,7	20,8	-12,1	-11,0	19,1	19,5
Pt-Dach-Cl	-7,4	-10,0	22,1	20,2	-9,1	-12,5	19,7	15,8
Pt-Dach-OH	-8,2	-7,3	21,3	21,5	-10,9	-7,1	17,1	20,2
JM118-Cl	-6,9	-7,9	23,5	22,8	-14,6	-9,0	13,8	18,8
JM118-OH	-9,3	-9,1	22,2	20,3	-13,0	-8,0	18,8	22,3
Pt-Pip-Cl	-5,8	-5,1	28,4	27,5	-4,1	-3,8	28,3	27,9
Pt-Pip-OH	-5,8	-6,2	25,3	24,3	-5,5	-3,9	25,3	26,5
Pt-Tz-Cl	-7,0	-8,3	18,5	19,1	-8,8	-5,6	15,5	19,3
Pt-Tz-OH	-4,9	-7,7	21,6	20,0	-6,6	-3,4	18,2	22,1

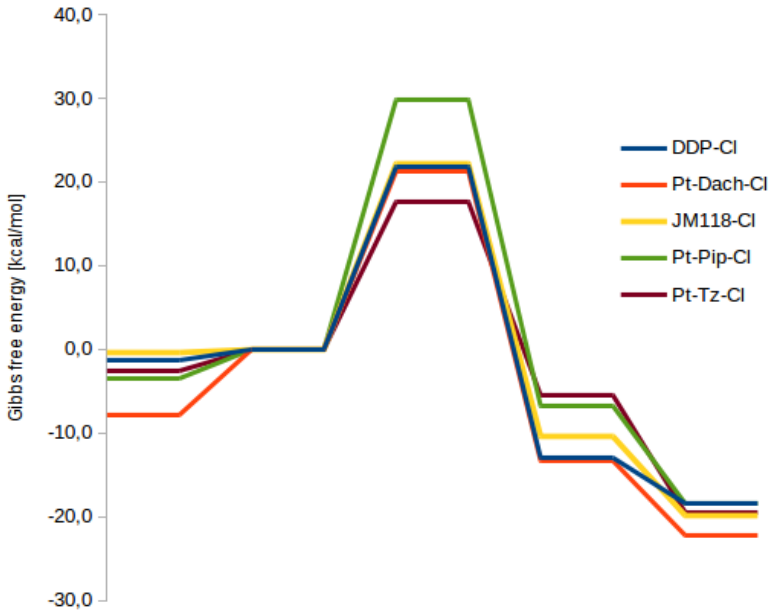

Figure 3.6: Gibbs free energy profiles of reactions of semi-hydrated Pt(II) complexes with guanine resulting from 6-311++G(2df,2pd) single point calculations in IEF-PCM.

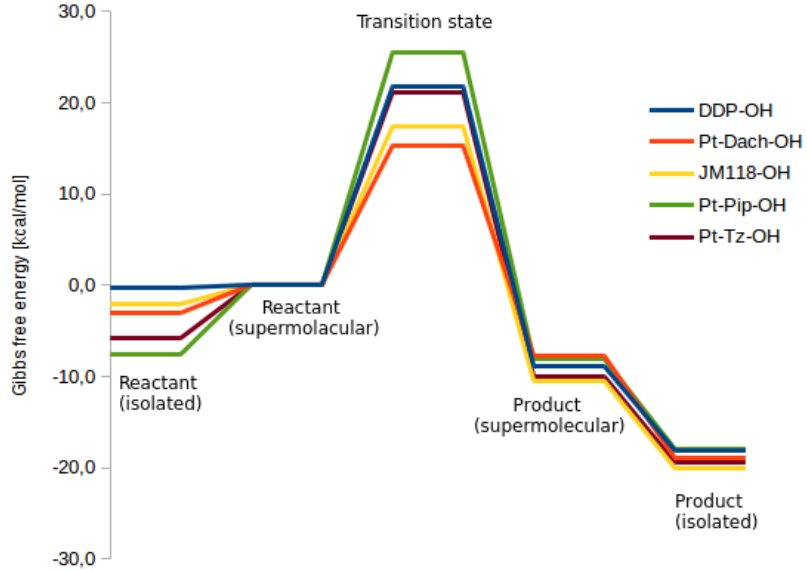

Figure 3.7: Gibbs free energy profiles of reactions of fully-hydrated Pt(II) complexes with guanine resulting from 6-311++G(2df,2pd) single point calculations in IEF-PCM.

Table 3.4: Rate constants [$M^{-1}s^{-}1$] of the reaction of Pt(II) complexes and guanine at 298,15 K resulting from 6-311++G(2df,2pd) single point calculations in IEF-PCM and in vacuum.

Complex	IEF-PCM	Vacuum
	$k(298,15)$ $[M^{-1}s^{-1}]$	$k(298,15)$ $[M^{-1}s^{-1}]$
DDP-Cl	6,17E+19	5,56E+22
DDP-OH	2,25E+19	4,08E+23
Pt-Dach-Cl	3,75E+22	1,30E+25
Pt-Dach-OH	2,66E+18	1,26E+21
JM118-Cl	2,52E+20	1,69E+21
JM118-OH	2,81E+20	7,77E+21
Pt-Pip-Cl	6,28E+17	2,27E+21
Pt-Pip-OH	4,92E+18	3,23E+16
Pt-Tz-Cl	6,36E+16	3,97E+16
Pt-Tz-OH	1,30E+20	1,05E+18

of JM118 complexes were in two cases slightly above the corresponding cisplatin complexes.

The lowest Gibbs free energy of activation, $\Delta G^{\ddagger} = 15{,}3$ kcal/mol was obtained for the Pt-Dach-OH complex. Generally, the complexes with Cl^- ligand had higher activation barriers in comparison with the complexes containing the OH^- ligand. The only exception were the complexes with thiazole. The highest activation barrier, $\Delta G^{\ddagger} = 29{,}9$ kcal/mol was obtained for the Pt-Pip-Cl complex.

According to the Hammond's postulate, we can relate the structure of transition state and the reaction energies. For exothermic reaction, if the absolute value of the activation energy is small in comparison with the reaction energy, the structure of the transition state resembles more closely the reactant structure. If the energies are the same, none of the reactant and product is better structural model for the transition state. The latter can be seen from the Figures 3.6 and 3.7.

From the graphs we can see that the isolated structures have lower values of Gibbs free energies in comparison with the supermolecular structures. That can be caused by the solvent environment, which stabilizes the isolated structures. Next, if we would consider the electronic energy, where is not included the entropic term, the values of the isolated complexes would probably be above the supermolecular structures.

The energies from the optimization calculations are included for orientation in Table 3.3. They are less exact than the energies obtained from the single point calculations with more precise basis set. Generally, the energetic trends resulting from the optimization calculations are similar with the trends resulting from the single point calculations. However, the optimization calculations yield lower energies of reactions.

Generally, both of the Tables 3.2 and 3.3 show, that the energetic values computed in vacuum are more spread than for the case of the IEF-PCM model. The IEF-PCM model stabilizes the structures and specific interactions within the system influence the energies less than in vacuum.

The determined rate constants in Table 3.4 reflect the heights of the activation barriers. The lower is the activation barrier, the higher is the rate constants, and according to the equilibrium Boltzmann distribution, that can be compensated for by a lower concen-

tration of reactant. The activities of the complexes as potential drugs can reflect the rates of the reactions. Similar rate to DDP-Cl has JM118-Cl, therefore it may exhibit similar properties to those of cisplatin. The reaction rates for the Pt(II) complexes with chloride can be ordered: Pt-Tz-Cl < Pt-Pip-Cl < DDP-Cl < JM118-Cl < Pt-Dach-Cl. The reaction rates for the Pt(II) complexes containing OH^- were relatively similar to each other, however, can be ordered: Pt-Dach-OH < Pt-Pip-OH < DDP-OH < Pt-Tz-OH < JM118-OH.

3.1.3 Bonding and association energies

Bonding (BE) energies for the isolated reactants and products are included in Table 3.5.

The more negative is the BE value, the stronger is the corresponding bond. The strength of the bond can be directly related to the bond distance.

Table 3.5 shows that the structures with the dach ligand had about twice as large BE between Pt and the dach ligand. That was due to the fact that both of the bonds between Pt and dach were included in the values.

The most stable of all of the Y ligands were piperidine and dach with the most negative value of BE, considering both the reactants and products. Next, JM118 was relatively strongly bound. Thiazole was bound relatively weakly, its BE values were comparable to the NH_3 ligand of cisplatin, however, generally, the absolute values of BE of thiazole were a bit larger.

The most stable ligands from all of the structures were the OH^- ligands. Next, the strength of the bonds between Pt and Cl^- was lower than between OH^- and Pt. Due to the same reason why the hydration reaction proceeded, the Cl^- was more likely to be substituted, whereas, the OH^- ligand was more strongly bound.

Next, we can see that the structures with the Cl^- ligand had higher absolute values of BE in comparison with the structures with the OH^- ligand. That corresponds to the lower values of BE between the Pt and Cl^- as well as with the longer bond lengths.

Association/bonding energies (BE) for the supermolecular structures of reactants, transition states and products for replacing the water with guanine are included in Table 3.6.

Table 3.6 shows that water in the reactant associates structures

Table 3.5: Bonding energies BE [kcal/mol] for isolated reactants and products of reactions of Pt(II) complexes with guanine (B3LYP/6-311++G(2df,2pd), IEF-PCM).

Complex	Cl/OH	H_2O/G	Y	NH_3
Reactants				
DDP-Cl	-54,7	-31,6	-50,2[a]	-61,6
DDP-OH	-82,9	-28,9	-49,6[a]	-60,8
Pt-Dach-Cl	-57,1	-32,5	-144,8	-
Pt-Dach-OH	-87,9	-28,7	-134,0	-
JM118-Cl	-64,3	-27,2	-54,9	-53,9
JM118-OH	-89,8	-31,0	-54,4	-62,1
Pt-Pip-Cl	-65,3	-38,5	-76,7	-58,1
Pt-Pip-OH	-90,5	-28,8	-66,7	-49,3
Pt-Tz-Cl	-70,2	-31,9	-51,9	-55,6
Pt-Tz-OH	-99,1	-29,8	-49,1	-51,9
Products				
DDP-Cl	-50,8	-52,2	-51,8[a]	-48,9
DDP-OH	-70,1	-49,0	-48,9[a]	-45,0
Pt-Dach-Cl	-52,5	-55,5	-130,4	-
Pt-Dach-OH	-78,4	-50,7	-117,9	-
JM118-Cl	-57,2	-56,8	-59,8	-53,6
JM118-OH	-85,8	-51,8	-55,4	-48,9
Pt-Pip-Cl	-57,0	-55,1	-60,3	-53,9
Pt-Pip-OH	-83,3	-49,8	-55,6	-47,0
Pt-Tz-Cl	-60,9	-56,6	-49,3	-56,9
Pt-Tz-OH	-89,7	-51,2	-44,6	-53,4

[a] NH_3 ligand of Pt

Table 3.6: Association/bonding energies (BE) [kcal/mol] for supermolecular structures of reactants, transition states and products for replacing water with guanine in reactions of Pt(II) complexes with guanine (B3LYP/6-311++G(2df,2pd), IEF-PCM).

	Reactants		TS		Products	
Complex	G	H_2O	G	H_2O	G	H_2O
DDP-Cl	-18,1	-35,9	-17,2	-2,7	-53,9	-7,4
DDP-OH	-15,5	-35,8	-15,6	-2,4	-52,5	-8,5
Pt-Dach-Cl	-24,1	-43,3	-16,0	-1,4	-64,7	-9,6
Pt-Dach-OH	-20,0	-39,4	-11,8	-3,7	-55,4	-7,7
JM118-Cl	-20,3	-40,9	-13,4	-1,9	-66,1	-9,6
JM118-OH	-18,5	-40,1	-13,9	-7,8	-53,4	-10,0
Pt-Pip-Cl	-23,6	-43,7	-15,4	-5,5	-53,5	-9,8
Pt-Pip-OH	-20,3	-42,7	-17,1	-5,3	-49,8	-9,4
Pt-Tz-Cl	-26,8	-45,5	-18,8	-8,2	-62,7	-6,5
Pt-Tz-OH	-22,3	-39,6	-16,0	-4,7	-59,9	-9,3

is more weakly bound to the Pt than guanine in the product associates. That is in agreement with the bond lengths discussed above. The bonding energies of both of the exchanging ligands in the transition states are lower in comparison with the association energy of the corresponding H-bonded molecules. That could be supported by the fact that generally, the bond lengths corresponding to the exchanging ligands in the transition states were about 0,5 Å longer than an average H-bond.

On average, the BE corresponding to water in coordinate covalent bonds with Pt are 5 times stronger in comparison with the associated water. For guanine, the BE are almost 3 times stronger. Guanine is stabilized in the associated state well, usually, it creates three H-bonds with the Pt(II) complex.

Different coordinations of guanine to the Pt(II) complexes in reactant associates structures were optimized in order to find the most convenient arrangement from the energetic point of view. Generally, the coordination of guanine was driven by the electrostatics. Often, guanine created H-bonds between its N7 and O6 atoms and both of the H atoms of water; and between its O6 atom and a polarized H atom bound to N atom of the Y ligand. For the complexes containing thiazole, N atom of the thiazole ligand was without H atoms, therefore the H-bond was created with the NH_3 ligand of Pt. Exceptions were the complexes with piperidine, where the guanine was stabilized with H-bonds between its N7 atom and the H atom bound to the N atom of piperidine and between its O6 atom and the NH_3 ligand of Pt.

Analogous procedure was carried out for the water molecule in the product associate structures. Again, the electrostatics was the principal effect. For the structures with Cl^- ligand, the water molecule was stabilized by H-bonds between adjacent NH and NH_3 groups of guanine. An exception was the structure with piperidine, where the water was stabilized between the H atom bound to the N atom of piperidine and the NH_3 ligand of Pt. Also, the global minimum for cisplatin was different, the water was stabilized between both of the NH_3 ligands of Pt. The latter mentioned exceptions contained two sterically adjacent amino groups bound to Pt and coordinated in a convenient way for the water molecule, which was not the case of the rest of the structures.

For product associate structures with OH^- ligand of Pt, water

was the most conveniently placed between the OH^- ligand and the adjacent H atom bound to N atom of another ligand. The only exception was the structure with thiazole, where the global minimum of water was between the H2 of N2 of amino group on guanine and the H1 of N1 of guanine, as it was in the case of the corresponding structure containing the Cl^- ligand. The OH^- group was already H-bonded to a near H atom of the thiazole ligand.

3.1.4 Electron density analysis

NBO analysis

NBO partial charges of molecular units of the isolated structures of reactants and products and are included in table 3.7.

Table 3.7 shows that the Pt atom had always relatively large positive value of the charge. It indicated the extent of electron donation from its ligands. Next, the charge of Pt was larger for the complexes with the OH^- ligand in comparison with the complexes with the Cl^- ligand. That indicated that the donation was larger from OH^- than from Cl^-. That could correspond with the electronegativity, O atom has larger electronegativity than the Cl atom, therefore the O atom attracted the Pt electrons more than the Cl and as the result, the Pt could have larger positive charge.

The dach ligand had the highest positive charge from the Y ligands. It was due to the fact that there were two bonds with the Pt atom and two electron pairs were included in two coordinate covalent bonds. Next, relatively high value of charges (both for products and reactants) had the piperidine ligand, followed by the JM118, cisplatin and the lowest charges had the thiazole ligand. The different charges corresponded to the different extent of electron donation from the various Y ligands. This trends corresponded to the trend obtained from the analysis of the bonding energies. The larger was the absolute value of the BE, the larger positive charge had the ligand.

NBO partial charges of molecular units of the supermolecular structures of reactants, transition states and products are included in table 3.8.

Tables 3.7 and 3.8 show that the charges of the listed molecular units follow the same trend. Usually, the difference is less than 0,03

Table 3.7: NBO partial charges [e] for molecular units of the isolated structures of reactants and products of reactions of Pt(II) complexes with guanine (B3LYP/6-311++G(2df,2pd), IEF-PCM).

Complex	Pt	Cl/OH	H_2O/G	Y	NH_3
Reactants					
DDP-Cl	0,68	-0,60	0,21	0,33[a]	0,38
DDP-OH	0,75	-0,59	0,19	0,29[a]	0,36
Pt-Dach-Cl	0,67	-0,61	0,20	0,73	-
Pt-Dach-OH	0,75	-0,60	0,18	0,67	-
JM118-Cl	0,67	-0,60	0,19	0,32	0,37
JM118-OH	0,75	-0,60	0,19	0,30	0,36
Pt-Pip-Cl	0,68	-0,59	0,21	0,40	0,31
Pt-Pip-OH	0,75	-0,59	0,19	0,30	0,35
Pt-Tz-Cl	0,67	-0,48	0,18	0,29	0,34
Pt-Tz-OH	0,78	-0,52	0,17	0,25	0,32
Products					
DDP-Cl	0,64	-0,60	0,31	0,32[a]	0,33
DDP-OH	0,72	-0,60	0,29	0,28[a]	0,32
Pt-Dach-Cl	0,65	-0,61	0,30	0,67	-
Pt-Dach-OH	0,72	-0,61	0,28	0,61	-
JM118-Cl	0,65	-0,60	0,30	0,34	0,31
JM118-OH	0,72	-0,60	0,28	0,33	0,27
Pt-Pip-Cl	0,65	-0,60	0,31	0,34	0,31
Pt-Pip-OH	0,72	-0,60	0,28	0,33	0,28
Pt-Tz-Cl	0,66	-0,55	0,29	0,27	0,33
Pt-Tz-OH	0,75	-0,58	0,23	0,25	0,31

[a] NH_3 ligand of Pt

Table 3.8: NBO partial charges [e] for molecular units of the supermolecular structures of reactants, transition states and products of reactions of Pt(II) complexes with guanine (B3LYP/6-311++G(2df,2pd), IEF-PCM).

Complex	Pt	Cl/OH	H_2O	G	Y	NH_3
Reactants						
DDP-Cl	0,67	-0,60	0,13	0,12	0,32[a]	0,35
DDP-OH	0,75	-0,61	0,15	0,10	0,26[a]	0,34
Pt-Dach-Cl	0,67	-0,61	0,13	0,11	0,70	-
Pt-Dach-OH	0,72	-0,61	0,13	0,11	0, 66	-
JM118-Cl	0,65	-0,53	0,14	0,13	0,35	0,26
JM118-OH	0,72	-0,60	0,14	0,11	0, 36	0,27
Pt-Pip-Cl	0,67	-0,61	0,13	0,13	0,38	0,30
Pt-Pip-OH	0,74	-0,62	0,12	0,11	0, 37	0,28
Pt-Tz-Cl	0,70	-0,53	0,14	0,11	0,27	0,32
Pt-Tz-OH	0,76	-0,55	0,13	0,10	0, 26	0,31
Transition states						
DDP-Cl	0,75	-0,60	0,05	0,13	0,31[a]	0,36
DDP-OH	0,83	-0,60	0,05	0,11	0,26[a]	0,35
Pt-Dach-Cl	0,74	-0,62	0,07	0,11	0,70	-
Pt-Dach-OH	0,82	-0,60	0,04	0,10	0,64	-
JM118-Cl	0,73	-0,54	0,07	0,12	0,36	0,26
JM118-OH	0,80	-0,59	0,05	0,08	0,29	0,37
Pt-Pip-Cl	0,76	-0,61	0,09	0,08	0,34	0,35
Pt-Pip-OH	0,81	-0,59	0,04	0,09	0,29	0,35
Pt-Tz-Cl	0,79	-0,56	0,06	0,13	0,26	0,32
Pt-Tz-OH	0,85	-0,53	0,03	0,11	0,24	0,30
Products						
DDP-Cl	0,63	-0,61	0,05	0,30	0,31[a]	0,32
DDP-OH	0,72	-0,58	-0,02	0,29	0,29[a]	0,30
Pt-Dach-Cl	0,64	-0,61	0,04	0,26	0,66	-
Pt-Dach-OH	0,73	-0,59	-0,04	0,27	0,63	-
JM118-Cl	0,64	-0,60	0,04	0,26	0,34	0,31
JM118-OH	0,73	-0,58	-0,02	0,28	0,31	0,29
Pt-Pip-Cl	0,64	-0,61	0,05	0,30	0,32	0,30
Pt-Pip-OH	0,72	-0,58	-0,02	0,29	0,31	0,29
Pt-Tz-Cl	0,67	-0,57	0,02	0,28	0,27	0,33
Pt-Tz-OH	0,75	0,58	0,04	0,23	0,25	0,31

[a] NH_3 ligand of Pt

e. The only exception is water in the reactants, its charge is about 0,07 e smaller for the supermolecular structures then for the isolated structures. Water in the supermolecular structures is involved in H-bonds with guanine, charge transfer between the water and guanine occurs and therefore, the total charge of water is lower. The sum of the charges of the water and guanine in supermolecular structures of reactants in only about 0,05 e more than the charge of water in isolated reactants (about 0,2 e). H-bonds of water in the supermolecular structures of products don't have such influence on the total charge of the guanine, because guanine is already surrounded by water from the solvent model.

The water in the reactants bears larger positive charge than in products, where it is associated with the Pt(II) complex. For the transition states, the values of the charge are in the middle. When the water is bound to the Pt, it donates the lone electron pair from O atom to the Pt atom, forming coordinate covalent bond. Analogously, it applies to the guanine which bears larger positive charge in products than in reactants. However, the charges of guanine in the transition states are close to the values in the reactants.

The changes of the charges of water and guanine in the supermolecular structures correspond to the changes of the charges of Pt.

AIM analysis

AIM analysis of electron density in important BCPs of the isolated structures of reactants and products of reactions of Pt(II) complexes with guanine is shown in Table 3.9.

In Table 3.9, it is possible to distinguish coordinate covalent bonds between Pt and its ligands.

It was confirmed that the Pt-Y bonds in reactants were stronger than Pt-O(H_2O) bonds in products. The trend in the BCPs of the Y ligands is similar to the trend observed at the NBO analysis and at the analysis of the bonding energies. The BCPs for the structures with the thiazole ligand are relatively high in comparison with the rest of the structures. An exception is water in reactants and guanine in products, respectively, of the structures with thiazole, their corresponding BCPs are relatively low. That is in agreement with the trans influence effect explained above. The exchanging ligands

Table 3.9: AIM analysis of electron density [10^{-2}e/Å^3] in important BCPs of the isolated structures of reactant and products of reactions of Pt(II) complexes with guanine (B3LYP/6-311++G(2df,2pd), IEF-PCM).

Complex	Cl/O(OH)	O(H_2O) /N7(G)	N(Y)	N(NH_3)
Reactants				
DDP-Cl	8,38	8,47	11,27[a]	12,48
DDP-OH	12,46	8,77	10,41[a]	12,32
Pt-Dach-Cl	8,65	8,52	11,66; 12,87	-
Pt-Dach-OH	12,30	8,80	10,93; 12,61	-
JM118-Cl	8,47	8,21	12,54	11,24
JM118-OH	12,42	8,82	10,70	12,41
Pt-Pip-Cl	8,63	8,25	12,63	11,27
Pt-Pip-OH	12,65	8,49	12,62	10,32
Pt-Tz-Cl	10,68	7,52	12,30	11,52
Pt-Tz-OH	14,36	7,12	12,12	11,56
Products				
DDP-Cl	8,21	11,63	11,38[a]	11,45
DDP-OH	12,24	11,63	10,65[a]	11,58
Pt-Dach-Cl	8,29	11,52	11,94; 11,94	-
Pt-Dach-OH	12,18	11,60	11,12; 11,86	-
JM118-Cl	8,44	11,58	11,49	11,52
JM118-OH	12,35	11,51	11,68	10,71
Pt-Pip-Cl	8,36	11,50	11,29	11,50
Pt-Pip-OH	12,60	11,54	11,63	10,21
Pt-Tz-Cl	9,31	10,53	11,37	11,50
Pt-Tz-OH	13,11	10,53	11,47	11,97

[a] NH_3 ligand of Pt

are in trans-position to the Cl^- and OH^- ligand, respectively.

The BCPs between Pt and Cl^- were almost $4{\cdot}10^{-2}$e/Å^3 smaller than for the OH^- ligands.

AIM analysis of electron density in important BCPs of the supermolecular structures of reactants, transition states and products of reactions of Pt(II) complexes with guanine is shown in Table 3.10.

Table 3.10 shows that for the transition states, there were found BCPs with relatively small values for the case of exchanging ligands.

The BCPs corresponding to water in isolated structures of reactants is about $1{\cdot}10^{-2}$e/Å^3 smaller than for the supermolecular structures of reactants. In supermolecular structures, the water is polarized due to the hydrogen bonds and the electron density is moved into the bond. That is analogous trend to the trend discussed for the NBO analysis. Similarly, it was not observed any significant difference in the BCP values for the case of guanine in products.

Table 3.10: AIM analysis of electron density [10^{-2}e/Å^3] in important BCPs of the supermolecular structures of reactant, transition states and products of reactions of Pt(II) complexes with guanine (B3LYP/6-311++G(2df,2pd), IEF-PCM).

Complex	Cl/O(OH)	O(H_2O)	N7(G)	N(Y)	N(NH_3)
Reactants					
DDP-Cl	8,36	9,55	-	11,46[a]	11,97
DDP-OH	12,32	9,23	-	12,04[a]	12,18
Pt-Dach-Cl	8,46	9,25	-	11,73; 12,50	-
Pt-Dach-OH	12,51	9,24	-	10,98; 12,68	-
JM118-Cl	9,28	9,34	-	12,01	10,84
JM118-OH	12,39	9,51	-	12,15	10,92
Pt-Pip-Cl	8,48	9,20	-	12,14	11,62
Pt-Pip-OH	12,42	9,05	-	12,42	10,57
Pt-Tz-Cl	9,87	8,85	-	12,14	11,49
Pt-Tz-OH	13,59	8,32	-	12,37	11,55
Transition states					
DDP-Cl	8,22	4,50	4,23	10,37[a]	12,04
DDP-OH	12,29	4,17	3,94	10,54[a]	12,38
Pt-Dach-Cl	8,16	4,12	4,04	12,28; 12,68	-
Pt-Dach-OH	11,76	4,14	3,95	11,38; 12,20	-
JM118-Cl	8,04	3,94	3,82	12,14	11,68
JM118-OH	11,76	4,20	3,07	11,12	12,72
Pt-Pip-Cl	8,25	4,42	3,80	11,47	12,13
Pt-Pip-OH	11,69	4,11	4,16	11,39	12,09
Pt-Tz-Cl	9,54	4,29	4,05	11,96	11,91
Pt-Tz-OH	12,83	3,89	3,63	12,02	11,94
Products					
DDP-Cl	8,08	-	11,49	10,75[a]	11,52
DDP-OH	11,46	-	11,57	10,64[a]	11,38
Pt-Dach-Cl	8,26	-	11,53	11,36; 11,96	-
Pt-Dach-OH	11,66	-	11,70	11,42; 11,82	-
JM118-Cl	8,42	-	11,67	11,45	11,58
JM118-OH	11,58	-	11,53	11,48	11,07
Pt-Pip-Cl	8,24	-	11,43	11,39	11,64
Pt-Pip-OH	11,97	-	11,58	11,34	10,50
Pt-Tz-Cl	9,38	-	11,09	11,77	11,91
Pt-Tz-OH	13,02	-	10,59	11,49	12,02

[a] NH_3 ligand of Pt

3.2 Reaction between the Ru(II) complex and guanine

As it was explained in the introduction chapter, the product of the hydration reaction, [Ru(II)(η^6-p-cymene(nalidixic acid)(H_2O)]$^{2+}$, is more reactive in comparison with the reactant of hydration reaction, which has the Cl^- ligand instead of the aqua-ligand. Therefore, it is willing to bind to the nucleophilic centra on biomolecules, particularly, the N7 position of guanine is preferred.

Two possible reaction pathways were considered, direct and indirect pathway to the N7 position of guanine. The indirect reaction mechanism was a two step mechanism, where first, a bond to the O6 position of guanine was created and from here the system rebound to the N7 atom. There were two energetic barriers with one intermediate state.

The reaction mechanism of the Ru(II) complex is relatively complex, in comparison, for example, to cisplatin where only the direct reaction mechanism proceeds.

All stationary points of the reaction, it means: reactant (R), intermediate state of indirect reaction mechanism bound to the O6 of guanine (I), and product bound to the N7 atom of guanine (P), were calculated, as it was described in the previous chapter. Transition state of the direct reaction mechanism (TS^D), as well as transition state of the indirect reaction mechanism between the reactant and intermediate state (TS^1) and between the intermediate state and product (TS^2), was calculated.

The nalidixic acid was bound to the Ru atom during the whole studied reaction of the Ru(II) complex and guanine.

In addition, structures with partially released p-cymene, in η^2-coordination, were optimized. Due to the η^2-coordination of p-cymene, free valences on Ru appeared, which were saturated with the O6 atom of guanine and water. This structure is labeled as P^{O6}, Figure 3.9.

The η^6-coordination of p-cymene was kept during the whole reaction, excluding the mentioned structure above, P^{O6}, which had different coordination of Ru ligands, while keeping the bond to the N7 guanine.

Schematic picture of the reaction pathway is shown in Figure 3.8.

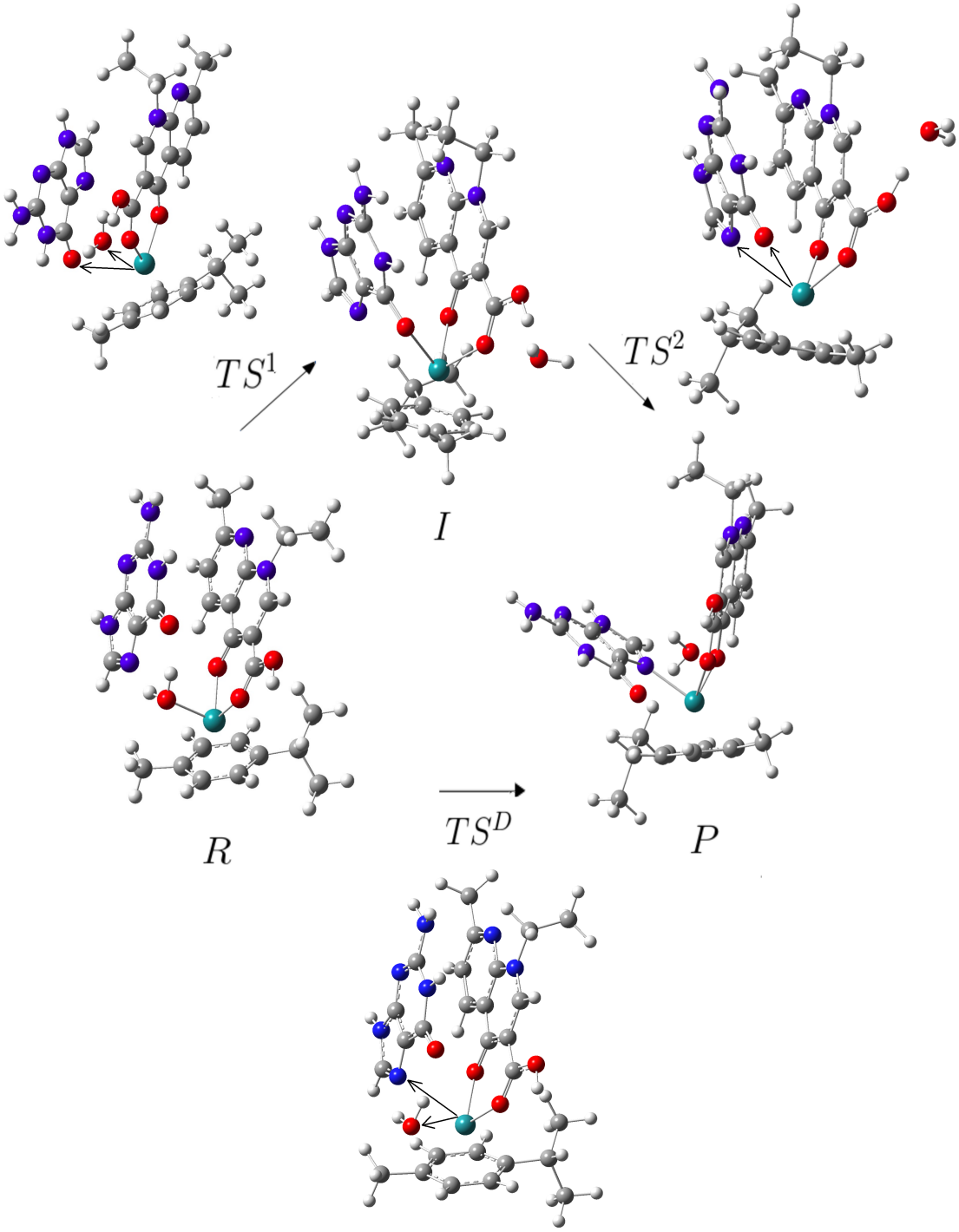

Figure 3.8: IEF-PCM B97D/6-31G* optimized stationary points of the reaction of the Ru(II) complex with guanine. The black arrows correspond to the anti-symmetric stretching movements.

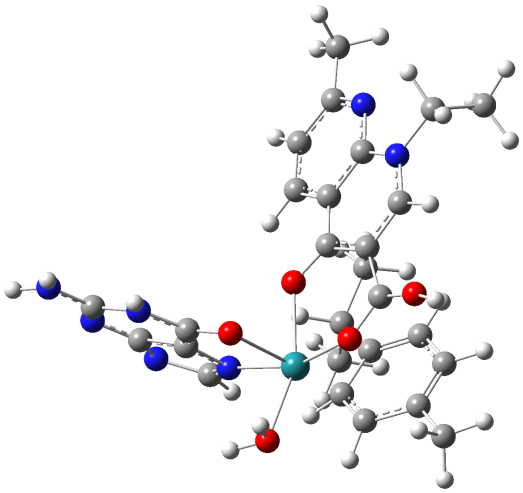

Figure 3.9: IEF-PCM B97D/6-31G* optimized P^{O6} structure.

3.2.1 Geometry parameters

Geometry parameters of all stationary points of the reaction resulting from IEF-PCM B97D/6-31G* calculations are shown in Table 3.11. These are bond lengths between Ru and water, distance between Ru and the middle of the p-cymene's 6-membered ring, and bond lengths between Ru and N7 and O6 atoms of guanine.

The bond length between the O of water ligand and Ru in the R structure is 0,1 Å shorter than the bond length between the O of the OH^- group of nalidixic acid and Ru in the I structure. That can be caused by the nucleophilic nature of the O6 of guanine in comparison with the O of water ligand, which is compensated with two H atoms.

Considering the Ru(II) complex bound to both of the N7 and O6 atoms of the guanine (P^{O6}) we can see that Ru was more closely bound to the N7 atom. That was in accordance with the priority in binding to the N7 atom in final product, which is well-established fact. Furthermore, that can indicate better stability of the P structure than I structure, which was confirmed in the energetic analysis below. The I and P structures show the same trend in the mentioned bond lengths, however, the difference is not that significant.

The released water molecule was always attached by hydrogen bonds to the OH^- group of nalidixic acid. Guanine in R structure was the most conveniently hydrogen bound with its O6 and N7 atoms to the water ligand. The mentioned interactions were driven by electrostatics.

Table 3.11: Geometry parameters [Å] of stationary points of the reaction of the Ru(II) complex with guanine in the IEF-PCM B97D/6-31G* computational model. The label Cym corresponds to the distance between Ru and the middle of the p-cymene's 6-membered ring.

Complex	**O(H_2O)**	**Cym**	**N7(G)**	**O6(G)**
R	2,15	1,74	3,92	4,10
I	5,11	1,76	3,61	2,16
P	4,75	1,76	2,12	3,54
P^{O6}	2,18	2,90	2,10	2,26
TS^D	3,14	1,75	2,88	4,08
TS^1	3,18	1,74	4,07	2,92
TS^2	6,45	1,74	3,01	2,95

Table 3.12: Gibbs free energies [kcal/mol] of the reaction of the Ru(II) complex with guanine in the IEF-PCM B97D/6-311++G(2df,2pd) computational model.

Reaction	ΔG	$\Delta G^{\ddagger}$
$R \rightarrow P$	-6,9	14,9
$R \rightarrow I$	2,3	15,9
$I \rightarrow P$	-9,2	16,1

3.2.2 Energy profile

Reaction energies, including the Gibbs free energy of reaction ΔG and free energy of activation $\Delta G^{\ddagger}$ are presented in Table 3.12. Gibbs free energy profile of the reaction pathway is shown in Figure 3.10.

Table 3.12 shows that the ΔG of product P was -6,9 kcal/mol, the reaction was spontaneous. The intermediate state was energetically above the reactant R, ΔG = 2,3 kcal/mol. The reaction barrier of the direct reaction mechanism was 1 kcal/mol lower in comparison with the indirect reaction barriers. Therefore, the reaction is more likely to proceed directly to the N7 atom of guanine.

The Gibbs free energy for the P^{O6} structure was 8,8 kcal/mol higher in comparison with the reactant R, which was energetically inconvenient.

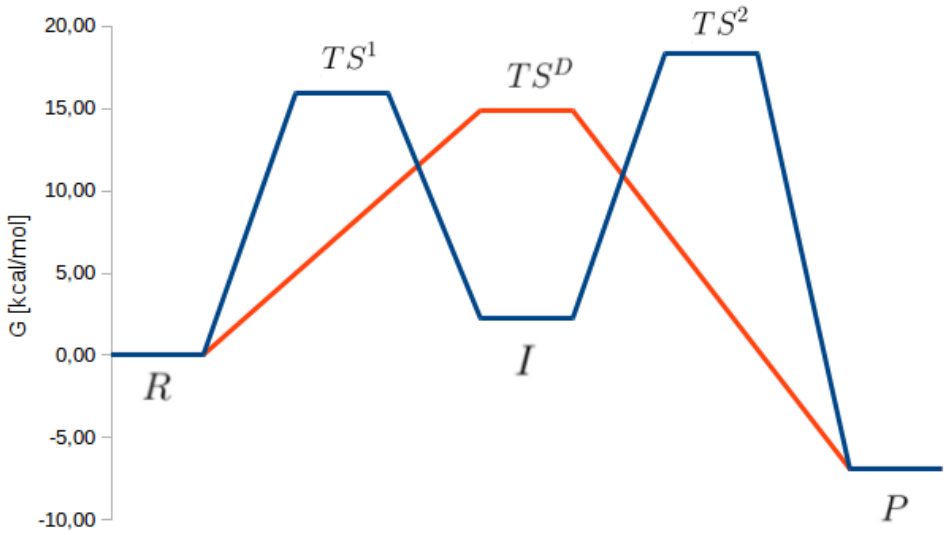

Figure 3.10: Gibbs free energy profile of the reaction of the Ru(II) complex with guanine in the IEF-PCM B97D/6-311++G(2df,2pd) computational model. Red curve corresponds to the direct reaction mechanism, blue curve corresponds to the indirect reaction mechanism.

3.2.3 Electron density analyses

Partial atomic charges obtained from NBO analysis of the structures are shown in Table 3.13.

The N7 atom of guanine was greater donor of electrons in comparison with the O6 atom of guanine. That can be seen on the charge of Ru, which was lower in the case where it was bound to N7. Also, it is supported by generally lower charges of N7 than O6. The charge on Ru was the highest in structure P^{O6} where both oxygen and nitrogen donated to Ru.

The charges of the N7 and O6 atoms of guanine were the less negative in the structures, where the atoms were bound to Ru. The difference was about 0,1 e. That was due to the fact that their negative charges were compensated by the coordinate covalent bond with the positively charged Ru. The analogous fact was valid for water, which was bound to Ru. It donated its free electron pair to the Ru and therefore its charge was less negative.

AIM analyses of structures of the reaction of the Ru(II) complex with guanine including bond critical points, BCP, between Ru and its ligands are shown in Table 3.14.

The values of electron density in BCP points indicate the strength of the interaction between the pairs of atoms. Also, the AIM anal-

Table 3.13: NBO charges [e] of stationary points of the reaction of the Ru(II) complex with guanine in the IEF-PCM B97D/6-311++G(2df,2pd) computational model.

Complex	**Ru**	**O(H_2O)**	**N7(G)**	**O6(G)**	**O(COOH)**	**O(keto)**
R	0,17	-0,82	-0,54	-0,67	-0,51	-0,52
I	0,17	-0,94	-0,49	-0,58	-0,54	-0,53
P	0,10	-0,95	-0,39	-0,69	-0,53	-0,57
P^{O6}	0,33	-0,81	-0,38	-0,56	-0,52	-0,49
TS^D	0,19	-0,95	-0,51	-0,67	-0,53	-0,54
TS^1	0,23	-0,95	-0,53	-0,67	-0,53	-0,54
TS^2	0,23	-0,94	-0,47	-0,60	-0,52	-0,54

Table 3.14: Electron density [10^{-2}e/Å^3] in chosen BCPs of stationary points of the reaction of the Ru(II) complex with guanine resulting from AIM analysis in the IEF-PCM B97D/6-311++G(2df,2pd) computational model.

Complex	**O(H_2O)**	**N7(G)**	**O6(G)**	**O(COOH)**	**O(keto)**
R	7,07	-	-	7,29	8,60
I	-	-	7,01	7,4	8,67
P	-	9,37	-	8,18	8,63
P^{O6}	6,36	8,97	5,57	9,17	9,3
TS^D	1,24	1,83	-	7,82	9,26
TS^1	1,07	-	1,36	8,30	9,55
TS^2	-	1,54	1,50	7,99	8,66

yses help to explain the topological changes that happen during the reaction. Generally, if the participating atoms were involved in another interaction as well, for example hydrogen bonding, the strength of the interaction between them was decreased, which resulted in lower number of electron density in corresponding BCP.

Table 3.14 shows that the N7 atom of guanine had greater electron density value in BCP than the O6 atom of guanine. That was valid even when comparing within one complex in the case of P^{O6} structure. This is in correspondence with the results from NBO analysis, the strength of the interaction between the N7 atom and Ru was greater in comparison with the O6 atom.

3.3 Binding of the Ru(II) complex to DNA

This section includes the results from the binding process of the Ru(II) complex to the DNA. Analogous procedure in relation to the Ru(II) QM calculations was carried out.

Also, bonding of the Ru(II) complex to both of the guanines was investigated. When referring to either the first or the second guanine, the guanine base of DNA at the 3' or 5' end of the DNA is referred. This is valid throughout the whole thesis.

All stationary points of the reaction, including reactant (R), intermediate states of indirect reaction mechanism bound either to O6 of the first or the second guanine (I^1, I^2), and two possible products bound to the N7 atom of one of the guanines (P^1 and P^2) were optimized. Transition states of the direct reaction mechanism (TS^{D-1}, TS^{D-2}), as well as transition states of the indirect reaction mechanism between the reactant and both of the intermediate states (TS^{1-1}, TS^{1-2}) and between the intermediate states and the corresponding products (TS^{2-1}, TS^{2-2}), were calculated.

Schematic pictures of QM calculated parts of the optimized structures on reaction pathway corresponding to bonding either to the first or second guanine, are shown in Figure 3.11 and in Figure .7.6 in attachment .7. The reactant is the same for the bonding either to the first or to the second guanine.

The direct reaction mechanism as well as the first step of the indirect reaction mechanism was always connected with the release of the water molecule bound to Ru, so a vacant position for a possible

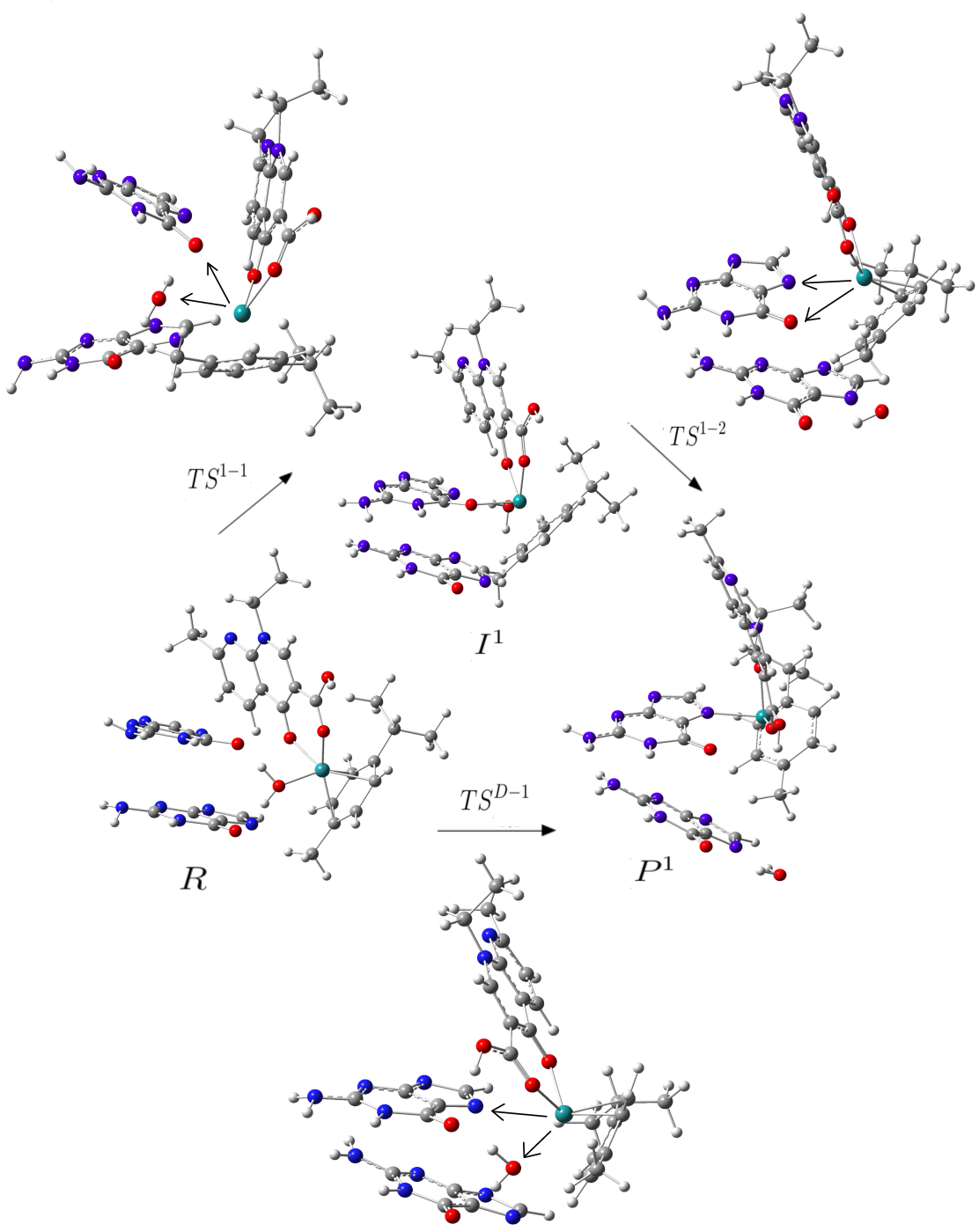

Figure 3.11: QM parts of ONIOM optimized stationary points of the reaction between the Ru(II) complex and the first guanine base of DNA. The black arrows correspond to the antisymmetric stretching movements.

bond with guanine was created. The η^6-coordination of p-cymene maintained during the whole reaction.

Also, structures connected with the dissociative mechanism were calculated, but it turned out that such structures were not stable enough within the used approach. For the dissociative mechanism, we supposed to have an additional intermediate state, where the water was already released from the Ru(II) complex, but the Ru(II) complex was not coordinated to the DNA oligomer yet. However, during optimizations, such structure bound either to the water again or to the N7 atom of one of the guanines. That could suggest that the reaction proceeded in the associative mechanism.

3.3.1 Geometry parameters

Relevant geometry parameters of all stationary points of the reaction resulting from ONIOM B97D/6-31G* calculations are shown in Table 3.15. These are bond lengths between Ru and water, distance between Ru and the middle of the p-cymene's 6-membered ring, and bond lengths between Ru and N7 and O6 atoms of both of the guanines.

Table 3.15 together with the Figure 3.11 show that the reactant R is stabilized due to hydrogen bonds between both of the H atoms of water and O6 atoms of both of the guanines. In the reactant R, the second guanine was closer to the Ru(II) complex in comparison with the first guanine. The distances could be influenced by the steric organization of DNA.

In both of the products, P^1 and P^2, the water molecule was released and the nalidixic acid and p-cymene were kept bound to the Ru atom.

In the transition states, where the aqua-ligand was exchanged with another ligand, the structure was always stabilized by hydrogen bonds between the aqua-ligand and both of the guanines. Generally, in transition states, the interchanging of the Ru(II) ligands was in the plane of the Ru atom and the participating guanine base.

Within the reaction, the Ru(II) complex was bound only to one of the guanines. If there was an interaction with the second guanine, it was mediated by hydrogen bonds of water.

The p-cymene ligand was the most closely bound to the Ru atom in reactants R. The N7 and O6 guanine atoms were bound to the

Table 3.15: Geometry parameters [Å] of stationary points of the reaction of the Ru(II) complex with B-DNA oligomer model in the ONIOM B97D/6-31G* computational model. The label Cym corresponds to the distance between Ru and the middle of the p-cymene's 6-membered ring.

Complex	**O(H_2O)**	**Cym**	**N7(G1)**	**O6(G1)**	**N7(G2)**	**O6(G2)**
R	2,09	1,74	5,08	4,00	4,52	4,13
I^1	3,70	1,82	3,96	2,12	4,70	4,23
I^2	5,94	1,78	7,55	5,15	3,96	2,19
P^1	6,53	1,75	2,15	3,88	5,59	5,95
P^2	4,48	1,74	6,89	5,10	2,18	3,73
TS^{D1}	2,69	1,74	2,98	4,23	4,56	4,94
TS^{D2}	2,41	1,74	5,33	3,87	2,59	4,06
TS^{1-1}	3,00	1,73	4,07	3,03	4,42	4,93
TS^{1-2}	3,52	1,77	7,54	4,99	4,29	2,90
TS^{2-1}	4,58	1,78	3,17	3,30	5,14	5,35
TS^{2-2}	4,77	1,75	6,82	5,06	3,02	2,83

Table 3.16: Gibbs free energies [kcal/mol] of the reaction of the Ru(II) complex with B-DNA oligomer model in the ONIOM B97D/6-31G* computational model.

Reaction	ΔG	$\Delta G^{\ddagger}$
$R \rightarrow P^1$	1,1	13,6
$R \rightarrow P^2$	-5,3	16,7
$R \rightarrow I^1$	7,6	23,2
$I^1 \rightarrow P^1$	-6,5	20,5
$R \rightarrow I^2$	12,3	22,6
$I^2 \rightarrow P^2$	-17,6	21,1

Ru atom more tightly than the water and therefore pushed the other atoms away a little.

The most likely, the water molecule created hydrogen bonds between both of the free O6 atoms of both of the guanines, if they were not included in any bond with the Ru(II) complex. As well, the water molecule created hydrogen bonds between the O6 and N7 atoms of guanine, which were not coordinated to the Ru(II) complex. The H atoms of water molecule bore partially positive charges due to the electronegativity difference between the H and O atoms. They were coordinated to the nucleofilic guanine atoms.

Comparing with the QM calculations we can see that the interaction of water with the OH− group of nalidixic acid was not that important here. Generally, the bond lengths obtained from the ONIOM calculations followed similar trends as in the case of the QM calculations. For example, the bond length between O of water and Ru in reactant is shorter than the bond lengths between O6 atoms of guanine and Ru in I^1 and I^2.

3.3.2 Energy profile

Energetic quantities of the reaction, including the Gibbs free energy of reaction ΔG and free energy of activation $\Delta G^{\ddagger}$ are presented in Table 3.16. Gibbs free energy profile of the reaction including both of the reaction pathways is shown in Figure 3.12.

The reaction of the Ru(II) complex with the first guanine was slightly endothermic process, ΔG = 1,1 kcal/mol. The reaction of

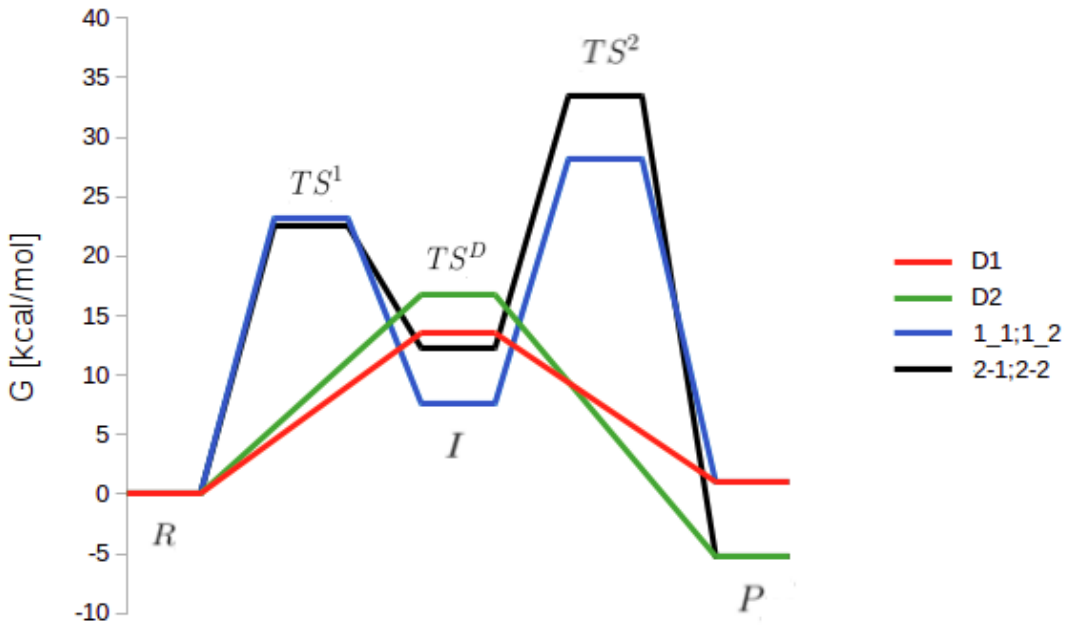

Figure 3.12: Gibbs free energy profile of the reaction of the Ru(II) complex with B-DNA oligomer model in the ONIOM B97D/6-31G* computational model. Red and green line, respectively, is the direct reaction pathway to the first and second guanine, respectively. Blue and black line, respectively, is the indirect reaction pathway to the first and second guanine, respectively.

the Ru(II) complex with the second guanine was was exothermic process, a spontaneous process from the thermodynamical point of view, ΔG = -5,3 kcal/mol. The direct reaction mechanism yielded smaller energy barrier in comparison with the indirect mechanism. That indicated that the direct mechanism was more likely to happen.

The first reaction barriers in the indirect reaction mechanisms differed by 0,6 kcal/mol with the preference for binding of the Ru(II) complex to the second guanine. However, the intermediate states in the indirect reaction mechanism differed by 4,7 kcal/mol, where the first guanine was energetically lower. The second reaction barrier in the indirect reaction mechanism differed for both of the reaction pathways by 5,3 kcal/mol, the barrier was lower for the case of the first guanine.

The lower reaction barrier in the case of the reaction pathway to the first guanine (for the direct and second step of the indirect reaction mechanism) suggested that the Ru(II) complex preferably bound to the first guanine. Also, that was supported by the fact that the highest BCP was found for the N7 atom of the first guanine (analysis below) and the bond length between Ru and N7 of the first guanine was shorter than in the case of the second guanine.

The reaction barriers, especially for the indirect mechanisms, were relatively high, that may be caused by the lack of solvent environment.

If we compare the energies with the energies obtained from QM calculations in the section above, the trends are similar. However, the reaction barriers for the indirect mechanism are about 7 kcal/mol lower in the case of the QM calculations. For both of the approaches, the direct mechanism yields the lowest reaction barriers. The ONIOM calculations result in lower barriers in the second step of the indirect reaction mechanism corresponding to the change between O6 and N7 on one guanine than the first reaction barrier in the indirect reaction mechanism corresponding to the transition from water to O6 of guanine. The difference was 2,8 and 1,5 kcal/-mol. However, in the case of the QM calculations, the barrier was 0,2 kca/mol higher.

Table 3.17: NBO charges [e] of stationary points of the reaction of the Ru(II) complex with B-DNA oligomer model in the ONIOM B97D/6-31G* computational model.

Complex	**Ru**	**O(H_2O)**	**N7(G1)**	**O6(G1)**	**N7(G2)**	**O6(G2)**
R	0,155	-0,824	-0,467	-0,638	-0,456	-0,622
I^1	0,177	-0,967	-0,514	-0,534	-0,444	-0,558
I^2	0,181	-0,940	-0,418	-0,632	-0,450	-0,542
P^1	0,096	-0,836	-0,405	-0,586	-0,481	-0,535
P^2	0,119	-0,984	-0,499	-0,616	-0,407	-0,571
TS^{D1}	0,231	-0,878	-0,484	-0,683	-0,432	-0,553
TS^{D2}	0,128	-0,847	-0,480	-0,593	-0,460	-0,598
TS^{1-1}	0,236	-0,911	-0,525	-0,548	-0,490	-0,603
TS^{1-2}	0,209	-0,874	-0,478	-0,569	-0,475	-0,566
TS^{2-1}	0,228	-0,958	-0,444	-0,597	-0,509	-0,595
TS^{2-2}	0,198	-0,946	-0,444	-0,629	-0,447	-0,580

3.3.3 Electron density analyses

Partial atomic charges obtained from NBO analyses of the structures are shown in Table 3.17.

From the partial charges on the Ru we could see that N7 atoms were greater donors of electrons in comparison with O6 atoms, because Ru atom had greater positive charge in those structures, where N7 atoms were not bound to the Ru atom in comparison with those structures, where the N7 atoms were bound.

The absolute values of the charges of both of the O6 atoms were greater than the charges of N7 atoms. That could be related to the fact that O atom has larger electronegativity than N atom and therefore attracts the electrons more and has greater negative charge.

The water had the lowest negative charge in the reactants (R), where it was bound to Ru. That was due to the fact that it donated electron pair to the Ru vacant orbital. The same was valid for the N7 and O6 atoms, their partial charges were about 0,1 e less, when the atoms were bound to Ru.

Ru charges differed just a little in reactant R and in intermediate states I^1 and I^2, because in all of the mentioned structures, the

Table 3.18: Electron density [10^{-2}e/Å^3] in chosen BCPs of stationary points of the reaction of the Ru(II) complex with B-DNA oligomer model resulting from AIM analysis in the ONIOM B97D/6-31G* computational model.

Complex	**O(H_2O)**	**N7(G1)**	**O6(G1)**	**N7(G2)**	**O6(G2)**	**O(COOH)**	**O(keto)**
R	8,59	-	-	-	-	6,44	8,62
I^1	-	-	7,02	-	-	6,45	8,37
I^2	-	-	-	-	6,18	6,91	9,36
P^1	-	8,45	-	-	-	7,86	7,82
P^2	-	-	-	7,94	-	7,23	8,63
TS^{D1}	2,82	1,77	-	-	-	7,32	8,09
TS^{D2}	4,61	-	-	3,46	-	5,78	6,98
TS^{1-1}	1,69	-	1,1	-	-	6,91	8,49
TS^{1-2}	-	1,24	0,93	-	-	7,38	7,61
TS^{2-1}	1,86	-	-	-	1,44	7,76	9,61
TS^{2-2}	-	-	-	1,28	2,01	8,79	8,88

Ru(II) complex interacted with oxygen. On the contrary, in the Ru(II)-N7 adducts, the charge on Ru was significantly reduced by electron donation from nitrogen. Interaction with O6 and N7 atom, respectively, was apparent on charge increase of these nucleophilic binding sites in relevant structures.

AIM analyses of structures of the reaction of the Ru(II) complex with DNA including bond critical points, BCP, between Ru and its ligands are shown in Table 3.18.

Table 3.18 shows that the electron density value in critical points between Ru and N7 guanine atoms was greater than between Ru and O6 guanine atoms. That was in correspondence with the preferred N7 position in products and it was valid when comparing between various structures.

For the transition states, there was always a low value BCP point between Ru and the exchanging ligands. The BCPs between water and Ru in the case of the TS^{D1} and TS^{D2} structures were higher than the BCPs corresponding to water in the TS^{1-1} and TS^{2-1} structures. Also, this fact could be seen in the case of the QM calculations in the previous section. It corresponds to the shorter bond

lengths between water and Ru in the TS^{D1} and TS^{D2} structures in comparison with the TS^{1-1} and TS^{2-1} structures.

Conclusion

In the first part of the thesis, interactions of five Pt(II) complexes with the guanine were calculated. These were the 'certified' drug cisplatin, as the benchmark, and four potential anticancer drugs including $PtCl_2$(diaminocyclohexane), $PtCl_2(NH_3)$(cyclohexylamine) (JM118), cis-[$PtCl_2(NH_3)$(piperidine)] and trans-[$PtCl_2(NH_3)$(thiazole)].

The complexes were considered in their semi-hydrated (one chloride ligand substituted with water) and fully-hydrated (one chloride ligand substituted with water, and the second one substituted with OH^-) forms after they were activated by hydration reaction. The resulting complexes containing the aqua-ligand on Pt were more reactive and could further interact with guanine.

All the stationary points were optimized using the hybrid density functional B3LYP and 6-31+G(d) basis set. Single point calculations were performed on optimized structures with the B3LYP functional and 6-311++G(2df,2pd) basis set. Relativistic pseudopotentials from Stuttgart-Dresden laboratory and explicit basis sets, which were augmented for the single point calculations, were used for the Pt, Cl, and S atoms. All the calculations were performed first in vacuum. Then, the solvent effects were described using the IEF-PCM approach, where NBO partial charges were used for rescaling the atomic radii of Cl, O, and S atoms in cavity construction.

Geometry parameters were evaluated on optimized structures. Bonding and association energies were analyzed. Partial atomic charges of Pt and its ligands were obtained from NBO analysis in order to understand the electron distribution within the investigated systems. AIM analysis of electron density in bond critical points (BCPs) was performed in order to describe binding interactions between pairs of atoms and their strength.

Energetic quantities were computed for all the reactions of Pt(II) complexes with guanine. All the reactions were exothermic and therefore spontaneous from the thermodynamic point of view. Generally, the complexes with the Cl^- ligand had higher activation barriers in comparison with the complexes containing the OH^- ligand. The only exception were the complexes with the thiazole.

Also, the rates of the reactions were computed; they can reflect the activities of the complexes as potential drugs. The reaction

rates for the Pt(II) complexes with chloride can be ordered: Pt-Tz-Cl < Pt-Pip-Cl < JM118-Cl < DDP-Cl < Pt-Dach-Cl. And, for the Pt(II) complexes containing OH^- Pt-Pip-OH < Pt-Dach-OH < DDP-OH < Pt-Tz-OH < JM118-OH, however, here the differences were lower.

The second part of the thesis discovered the reaction of Ru(II) 'piano-stool' complex, [Ru(II)(η^6-p-cymene(nalidixic acid)(H_2O)]$^{2+}$, with guanine by employing QM computational method and after with DNA oligomer by employing QM/MM computational method. The Ru(II) complex was obtained as a product of hydration reaction, where the Cl^- ligand of the Ru atom was substituted with water, which activated the Ru(II) complex for the interaction with DNA.

The reactions of the Ru(II) complex with both guanine and DNA model, where the Ru(II)-N7 mono-adduct were created, were calculated. Both of the direct and indirect reaction mechanisms were calculated. Within the indirect mechanism, there is an extra intermediate state where the Ru(II) complex is bound to the O6 atom of guanine and from here it rebounds to the N7 guanine position.

The QM calculations were carried out using Gaussian software program. Optimizations of structures were performed using B97D functional with 6-31G* basis set, first, in vacuum and second, using IEF-PCM approach for the description of solvent effects. After, single point calculations were performed on optimized structures using 6-311++G(2df,2pd) basis set.

The QM/MM calculations were carried out using Gaussian software program with the ONIOM method, enabling combination of QM and MM approaches. The model consisted of the Ru(II) complex, DNA oligonucleotide including 16 base pairs and 28 neutralizing Na^+ ions. The calculations were performed in vacuum environment. Optimization calculations of all stationary points were performed at the B97D/6-31G* level of theory for the QM part of the system. The MM part of the simulated system was described with Amber force field.

The geometry of Ru and its ligands were analyzed for optimized structures. Thermodynamic parameters including the Gibbs free energies were evaluated. Analyses of electron density including NBO analysis of partial atomic charges and Bader's AIM analysis of electron density in critical points of electron density (BCP) of all sta-

tionary points of the reaction were performed.

From the QM calculations was obtained 14,9 kcal/mol high reaction barrier in the case of the direct reaction mechanism. The indirect mechanism yielded two reaction barriers: 16,1 and 15,9 kcal/-mol. The final product was stabilized with -6,9 kcal/mol. That indicated that the direct reaction mechanism was more likely to happen.

Regarding the ONIOM model, for the case of the bonding to the second guanine (at the 5' end of DNA), the reaction was an exothermic process, the reaction energy ΔG = -5,3 kcal/mol. For the case of the first guanine (at the 3' end of DNA), the reaction was slightly endothermic, the reaction energy ΔG = 1,1 kcal/mol. The intermediate states in the indirect reaction mechanism differed by 4,7 kcal/mol, where the first guanine was energetically lower.

The direct reaction mechanism yielded smaller energy barrier in comparison with the indirect mechanism. That could indicate that the direct mechanism was more likely to happen. $\Delta G^{\ddagger}$ values for the direct reaction mechanism were 13,6 and 16,7 kcal/mol, for the first and second guanine, respectively. The first reaction barriers for the indirect reaction mechanism were 23,2 and 20,5 kcal/mol.

In the indirect mechanism, there was only slight difference (0,6 kcal/mol) between both of the first reaction barriers. The second reaction barriers in the indirect mechanism differed by 5,3 kcal/mol, the barrier was lower for the case of the first guanine.

During the reaction, the water molecule was released and the nalidixic acid and p-cymene ligand of Ru were kept in their positions.

Bibliography

[1] Chebner, B.A., *Barnett Rosenberg: In Memoriam (1924-2009).* Cancer Res. 70, 1746-48 (2010)

[2] Perez, R.P., *Cellular and Molecular Determinants of Cisplatin Resistance.* Eur. J. Cancer 34, 1535-1542 (1998)

[3] National cancer institute, (2011)

[4] Lippert, B.A.,editor. *Cisplatin: Chemistry and Biochemistry of a Leading Anticancer Drug.* Wiley-VCH Verlag GmbH, Wienheim, Germany (1999)

[5] Bradáč, O., Zimmermann, T., Burda, J.V. *Copparison of the electronic properties, and thermodynamic and kinetics parameters of the aquation of selected platinum(II) derivatives with their anticancer IC_{20} indexes.* J. Mol. Model. 14, 705-716, (2008)

[6] Morris, R.E., Aird, R.E., Murdoch, P., Chen, H., Cummings, J., Hughes, N.D., Parsons, S., Parkin, A., Boyd, G., Jodrell, D.I., Sadler, P.J., *Inhibition of cancer cell growth by ruthenium(II) arene complexes.* J.Med.Chem. 44, 3616-21 (2001)

[7] Kljun, J., Bytzek, A.K., Kandioller, W., Bartel, C., Jakupec, M.A., Christian, G.H., Keppler, B.K., Turel, I., *Physicochemical Studies and Anticancer Potency of Ruthenium η^6-p-cymene Complexes Containing Antibacterial Quinolones.* Organometallic 30, 2506-2512 (2011)

[8] Futera, Z., Klenko, J., Sponer, J.E., Sponer, J., Burda, J.V., *Interactions of the "Piano-Stool" [ruthenium(II)(η^6-arene)(en)Cl]$^+$ Complexes with Water Nucleobases; Ab Initio and DTF Study.* J Comput Chem 30, 1758-1770 (2009)

[9] Futera, Z., Burda, J.V., *Reaction Mechanism of Ru(II) Piano-Stool Complexes: Umbrella Sampling QM/MM MD Study* J. Comp. Chem. 35, 1446-1456 (2014)

[10] Liu, H., Parkinson, J.A., Bella, J., Wang, F., Sadler, P.J., *Penetrative DNA Intercalation and G-base Selectivity*

of an Organometallic Tetrahydroanthracene Ru-II Anticancer Complex. Chem.Sci. 1(2), 258-270 (2010)

[11] Szabo, A., Ostlund, N.S., *Modern Quantum Chemistry - Introduction to Advanced Electronic Structure Theory.* New York: Dover Publications Inc. (1996)

[12] Skala, L., *Kvantova teorie molekul.* Prague: Karolinum (1995)

[13] Jensen, F., *Introduction to Computational Chemistry.* West Sussex: John Wiley & Sons, Ltd. (2007)

[14] Leach, A.R., *Molecular Modelling Principles and Application.* Essex: Longman imprint, 2nd ed. (2001)

[15] Thijssen, J., *Computational Physics* Cambridge: Cambridge University Press 2nd ed. (2007)

[16] Cramer, Ch.J., *Essentials of Computational Chemistry: Theories and Models.* West Sussex: John Wiley & Sons, Ltd. (2004)

[17] Rappe, A.K., Casewit, C.J., Colwell, K.S., Goddard, W.A.I., Skiff, W.M., *UFF, a full periodic table force field for molecular mechanics and molecular dynamics simulations.* J. Am. Chem. Soc. 114 (25), 10024-10035 (1992)

[18] Cornell, W.D.,Cieplak, P., Bayly, C., Gould, I.R., Merz,K.M.J., Ferguson, D.M., Spellmeyer, D.C., Fox, T., Caldwell, J.W., and Kollman, P.A, *A Second Generation Force Field for the Simulation of Proteins, Nucleic Acids, and Organic Molecules.* J. Am. Chem. Soc. 117, 5179-5197 (1995)

[19] Ochterski, J.W., *Thermochemistry in Gaussian.* The Official Gaussian Website, [Online] (2010) *http* : *//www.gaussian.com/g_whitepap/thermo.htm*

[20] Olander, D.R., *General Thermodynamics.* Boca Raton: CRC Press (2008)

[21] Forster, J.P., Weinhold, F., *Natural Hybrid Orbitals.* J . Am. Chem. Soc. 102, 7211-7218 (1980)

[22] Frisch, M. J., et al., *Gaussian 03, Revision C.02.* Wallingford CT: Gaussian, Inc.,Gaussian, Inc. (2004)

[23] Frisch, M. J., et al., *Gaussian 09, Revision D.01.* Wallingford CT: Gaussian, Inc.,Gaussian, Inc. (2009)

[24] Case, D.A., et al., *AMBER 8.* San Francisco: University of California (2004)

[25] Cossi, M., Scalmani, G., Rega, N., Barone, V., *New developments in the polarizable continuum model for quantum mechanical and classical calculations on molecules in solution.* J. Chem. Phys. 117, 43-54 (2002)

[26] Zimmermann, T., Burda, J.V., *Charge-scaled cavities in polarizable continuum model: Determination of acid dissociation constants for platinum-amino acid complexes.* J. Chem. Phys. 131, 135101-1 (2009)

[27] Keith, T.A., *AIMAll 11.08.23* Overland Park KS, USA: TK Gristmill Software (2011)

[28] Schaftenaar, G., Noordik, J.H., *Molden: a pre- and post-processing program for molecular and electronic structures.* J. Comput.-Aided Mol. Design 14, 123-134 (2000)

[29] Humphrey, W., Dalke, A., Schulten, K., *VMD - Visual Molecular Dynamics* J. Molec. Graphics 14, 33-38 (1996)

[30] Dennington, R., Keith, T., Millam, J., *GaussView, Version 5.* Semichem Inc., Shawnee Mission, KS, (2009)

[31] Grimme, S., *Semiempirical GGA-type Density Functional Constructed with a Long-range Dispersion Correction.* J. Comp. Chem. 27, 1787-99 (2006).

[32] Becke, A.D., *Density-functional thermochemistry. V. Systematic optimization of exchange-correlation functionals.* J. Chem. Phys. 107, 8554-8560 (1997)

[33] Ditchfield, R., Hehre W.J., Pople, J.A., *Self-Consistent Molecular-Orbital Methods. IX. An Extended Gaussian-Type Basis for Molecular-Orbital Studies of Organic Molecules.* J. Chem. Phys. 54(2), 724-728 (1971)

[34] Futera, Z., Sodeyama, K., Burda, J.V., Einaga, Y., Tateyama, Y., *Double-QM/MM Method for Investigating Donor-Acceptor Electron Transfer Reactions in Solution.* Phys. Chem. Chem. Phys. 16(36), 19530-39 (2014)

[35] Torigoe, H., Ono, A., Kozasa, T., *Hg^{II} Ion Specifically Binds with T:T Mismatched Base Pair in Duplex DNA.* Chem. Eur. J. 16, 13218-25 (2010)

List of Tables

3.1 The Pt-ligand bond lengths for the reactions of Pt complexes with guanine. 45
3.2 Reaction profile of reactions of Pt(II) complexes with guanine from single point calculations. 48
3.3 Reaction profile of reactions of Pt(II) complexes with guanine from optimization calculations. 48
3.4 Rate constants for reactions of Pt(II) complexes with guanine. 50
3.5 Bonding energies for isolated structures of reactions of Pt(II) complexes with guanine. 53
3.6 Association/bonding energies for replacing water with guanine in reactions of the Pt(II) complexes with guanine. 54
3.7 NBO analysis of isolated Pt(II) complexes interacting with guanine. 57
3.8 NBO analysis of Pt(II) supermolecular structures interacting with guanine. 58
3.9 AIM analysis of the isolated structures of reactions of Pt(II) complexes with guanine. 60
3.10 AIM analysis of the supermolecular structures of reactions of Pt(II) complexes with guanine. 62
3.11 Geometry parameters within the reaction of the Ru(II) complex and guanine. 66
3.12 Reaction profile of the reaction of the Ru(II) complex with guanine. 66
3.13 NBO analysis of the reaction of the Ru(II) complex and guanine. 68
3.14 AIM analysis of the reaction of the Ru(II) complex with guanine. 68
3.15 Geometry parameters of complexes of the reaction of the Ru(II) complex and DNA. 72
3.16 Reaction profile of the reaction of the Ru(II) complex with DNA. 73
3.17 NBO analysis of the reaction of the Ru(II) complex and DNA. 76

3.18 AIM analysis of the reaction of the Ru(II) complex with DNA. 77

List of Abbreviations

acac	acetylacetone
a.u.	atomic units
B3LYP	Becke three-parameter Lee-Yang-Parr hybrid exchange correlation functional
B97D	Grimme's functional including dispersion
BCP	Bond Critical Point
CC	Coupled Clusters
CI	Configuration Interaction method
Cym	P-cymene
DDP-Cl	Semi-hydrated cisplatin
DDP-OH	Fully-hydrated cisplatin
DFT	Density Functional Theory
DNA	Deoxyribonucleic acid
ECP	Effective Core Potentials
en	Ethylenediamine
FF	Force Field
G	Guanine
G1	The first guanine; guanine at the 3' end of DNA
G2	The second guanine; guanine at the 5' end of DNA
I	Intermediate state of the reaction of the Ru(II) complex with guanine
I^1	Intermediate state of the reaction of the Ru(II) complex with DNA bound to O6 atom of guanine at the 3' end of DNA
I^2	Intermediate state of the reaction of the Ru(II) complex with DNA bound to O6 atom of guanine at the 5' end of DNA
JM118-Cl	Semi-hydrated JM118
JM118-OH	Fully-hydrated JM118
LDA	Local Density Approximation
LCAO	Linear Combination of Atomic Orbitals
MD	Molecular Dynamics
MM	Molecular Mechanics
MP	Moller-Plesset method
NBO	Natural Bond Orbital analysis
NVT	Canonical ensemble

P	Product of the reaction of the Ru(II) complex with guanine
P^{O6}	Structure of the reaction of the Ru(II) complex with guanine where Ru is bound to both of the N7 and O6 atoms of guanine
P^1	Product of the reaction of the Ru(II) complex with DNA bound to N7 atom of the guanine at the 3' end of DNA
P^2	Product of the reaction of the Ru(II) complex with DNA bound to N7 atom of the guanine at the 5' end of DNA
PBC	Periodic Boundary Conditions
PP	Pseudopotentials
PT	Perturbation Theory
Pt-Dach-Cl	Semi-hydrated $PtCl_2$(diaminocyclohexane)
Pt-Dach-OH	Fully-hydrated $PtCl_2$(diaminocyclohexane)
Pt-Pip-Cl	Semi-hydrated cis-[$PtCl_2(NH_3)$(piperidine)]
Pt-Pip-OH	Fully-hydrated cis-[$PtCl_2(NH_3)$(piperidine)]
Pt-Tz-Cl	Semi-hydrated trans-[$PtCl_2(NH_3)$(thiazole)]
Pt-Tz-OH	Fully-hydrated trans-[$PtCl_2(NH_3)$(thiazole)]
QEq	Charge Equilibration method
QM	Quantum Mechanics
QM/MM	Combined Quantum Mechanics and Molecular Mechanics method
R	Reactant of the reaction of the Ru(II) complex with DNA
SCF	Self Consistent Field method
TS	Transition state
TS^D	Transition state in direct mechanism of the reaction of the Ru(II) complex with guanine
TS^{D-1}	Transition state in direct mechanism of the reaction of the Ru(II) complex with the first guanine of DNA
TS^{D-2}	Transition state in direct mechanism of the reaction of the Ru(II) complex with the second guanine of DNA
TS^1	First transition state in indirect mechanism of the reaction of the Ru(II) complex with guanine
TS^{1-1}	First transition state in indirect mechanism of the reaction of the Ru(II) complex with the first guanine of DNA

TS^{1-2}	First transition state in indirect mechanism of the reaction of the Ru(II) complex with the second guanine of DNA
TS^{2}	Second transition state in indirect mechanism of the reaction of the Ru(II) complex with guanine
TS^{2-1}	Second transition state in indirect mechanism of the reaction of the Ru(II) complex with the first guanine of DNA
TS^{2-2}	Second transition state in indirect mechanism of the reaction of the Ru(II) complex with the second guanine of DNA
UFF	Universal Force Field
X	Cl^{-}
Y	Diaminocyclohexane, cyclohexylamine, piperidine or thiazole ligand of Pt

Attachments

.1 Basis sets for Pt, Cl and S atoms used in QM optimizations.

```
Pt
 S   3   1.0
      16.559563        -.88494470
      13.892440         1.5011228
       5.8536080       -1.5529012
 S   1   1.0
       1.2873200         1.0000000
 S   1   1.0
        .60473200        1.0000000
 S   1   1.0
        .14278300        1.0000000
 S   1   1.0
        .50969000E-01    1.0000000
 S   1   1.0
        .15000000E-01    1.0000000
 P   2   1.0
       7.9251750         4.9530757
       7.3415380        -5.8982100
 P   2   1.0
       1.9125150         .30474250
       1.0715450         .71648940
 P   1   1.0
        .43791700        1.0000000
 P   1   1.0
        .93621000E-01    1.0000000
 P   1   1.0
        .27802000E-01    1.0000000
 D   4   1.0
       3.9395310        -.58264390
```

```
      3.5877770        .59225760
      1.2862310        .47369210
       .51981400        .57652020
 D   1    1.0
       .17471500        1.0000000
 D   1    1.0
       .50000000E-01    1.0000000
 F   1     1.0
       0.98035907       1.00


Cl
 S  3  1.0
    14.073076000     0.020345000
     2.331565000    -0.289223000
     0.507100000     0.630367000
 S  1  1.0
     0.182433000     1.000000000
 P  3  1.0
     3.353129000    -0.041552000
     0.785686000     0.399748000
     0.267454000     0.591829000
 P  1  1.0
     0.078275000     1.000000000
 P  1  1.0
    0.015477000     1.000000000
 D  1    1.0
    0.61834526     1.00


S    0
 S    3   1.00
         6.83351800           -0.438750000E-01
         2.07773800            0.319894000
```

```
      0.419121000          -0.661233000
 S    1   1.00
      0.153237000           1.00000000
 S    1   1.00
      0.0766200             1.00000000
 P    3   1.00
       1.81713900          -0.792270000E-01
      0.855070000           0.263671000
      0.312053000           0.580682000
 P    1   1.00
      0.101687000           1.00000000
 P    1   1.00
      0.298100000E-01       1.00000000
 P    1   1.00
      0.014900              1.00000000
 D    1   1.00
      0.49810406            1.0000
```

.2 Pseudopotentials on Pt, Cl and S atoms used in QM calculations.

```
PT   0
PT-ECP    5    60
H POTENTIAL
 1
2            1.00000000          0.00000000
S-H POTENTIAL
 2
2           13.42865100        579.22386100
2            6.71432600         29.66949100
P-H POTENTIAL
 2
2           10.36594400        280.86077400
2            5.18297200         26.74538200
D-H POTENTIAL
```

```
 2
2              7.60047900          120.39644400
2              3.80024000           15.81092100
F–H POTENTIAL
 1
2              3.30956900           24.31437600
G–H POTENTIAL
 1
2              5.27728900          −24.21867500



Cl  0
Cl_10_mwb    3    10
F
1
2            1.0000000            0.00000000
S − F
2
2            6.3943000           33.13663200
2            3.1971000           16.27072800
P − F
2
2            5.6207000           24.41699300
2            2.8103000            7.68305000
D − F
1
2            5.3381000           −8.58764900

S     0
S–ECP      3     10
F POTENTIAL
 1
2              1.00000000           0.00000000
S–F POTENTIAL
```

```
 1
2            3.74389164          37.97481900
P–F POTENTIAL
 1
2            3.08608744          18.79052931
D–F POTENTIAL
 1
2            4.86241400          −7.83796400
```

.3 Basis sets for Pt, Cl and S atoms used in QM single point calculations.

```
–Pt
 S   3   1.0
      16.559563          −.88494470
      13.892440           1.5011228
       5.8536080          −1.5529012
 S   1   1.0
       1.2873200           1.0000000
 S   1   1.0
        .60473200          1.0000000
 S   1   1.0
        .14278300          1.0000000
 S   1   1.0
        .50969000E−01      1.0000000
 S   1   1.0
        .15000000E−01      1.0000000
 S   1   1.0
        .07500000E−01      1.0000000
 P   2   1.0
       7.9251750           4.9530757
       7.3415380          −5.8982100
 P   2   1.0
       1.9125150           .30474250
       1.0715450           .71648940
```

```
 P   1    1.0
          .43791700          1.0000000
 P   1    1.0
          .93621000E-01      1.0000000
 P   1    1.0
          .27802000E-01      1.0000000
 P   1    1.0
          .13000000E-01      1.0000000
 D   4    1.0
        3.9395310         -.58264390
        3.5877770          .59225760
        1.2862310          .47369210
         .51981400         .57652020
 D   1    1.0
          .17471500          1.0000000
 D   1    1.0
          .50000000E-01      1.0000000
 D   1    1.0
          .25000000E-01      1.0000000
 F   1      1.0
      1.419333    1.00
 F   1      1.0
       .466239    1.00
 G   1      1.0
      1.207702    1.00


Cl
 S  3  1.0
     14.073076000      0.020345000
      2.331565000     -0.289223000
      0.507100000      0.630367000
 S  1  1.0
      0.3648000           1.00
S  1  1.0
```

```
     0.0912000          1.00
S  1  1.0
    0.0483000          1.00
 P  3  1.0
     3.353129000    -0.041552000
     0.785686000     0.399748000
     0.267454000     0.591829000
 P  1  1.0
     0.078275000     1.000000000
 P  1  1.0
     0.015477000     1.000000000
P  1  1.0
    0.0483000          1.00
 D      1  1.00
  0.1500000000D+01   0.1000000000D+01
 D      1  1.00
  0.3750000000D+00   0.1000000000D+01
 F      1  1.00
  0.7000000000D+00   0.1000000000D+01

 S    0
 S    3   1.00
        6.83351800          -0.438750000E-01
        2.07773800           0.319894000
        0.419121000          -0.661233000
 S    1   1.00
       0.153237000            1.00000000
 S    1   1.00
       0.070                  1.00000000
 P    3   1.00
        1.81713900          -0.792270000E-01
       0.855070000           0.263671000
       0.312053000           0.580682000
 P    1   1.00
```

```
      0.101687000            1.00000000
P     1    1.00
      0.298100000E-01        1.00000000
P     1    1.00
      0.100000000E-01        1.00000000
D     1    1.00
      2.7009         1.00
D     1    1.00
      0.2433         1.00
F     1    1.00
      0.6961         1.00
```

.4 Schematic pictures of the reactants, transition states and products of the reactions of the Pt(II) complexes in the fully-hydrated form with guanine

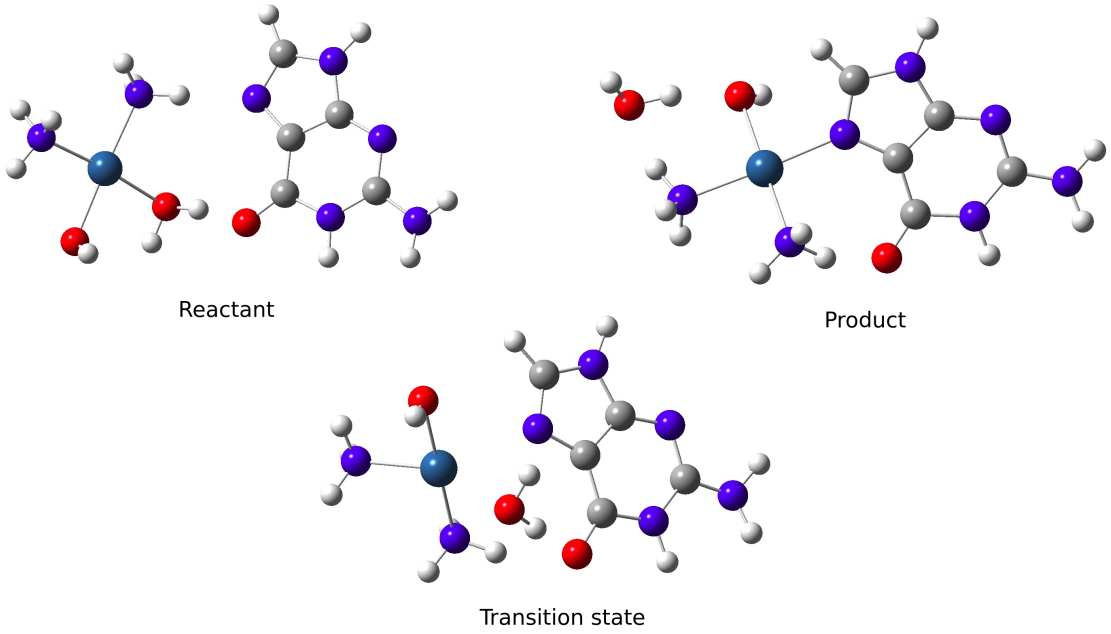

Figure .4.1: Reactant, transition state and product of reaction of DDP-OH with guanine.

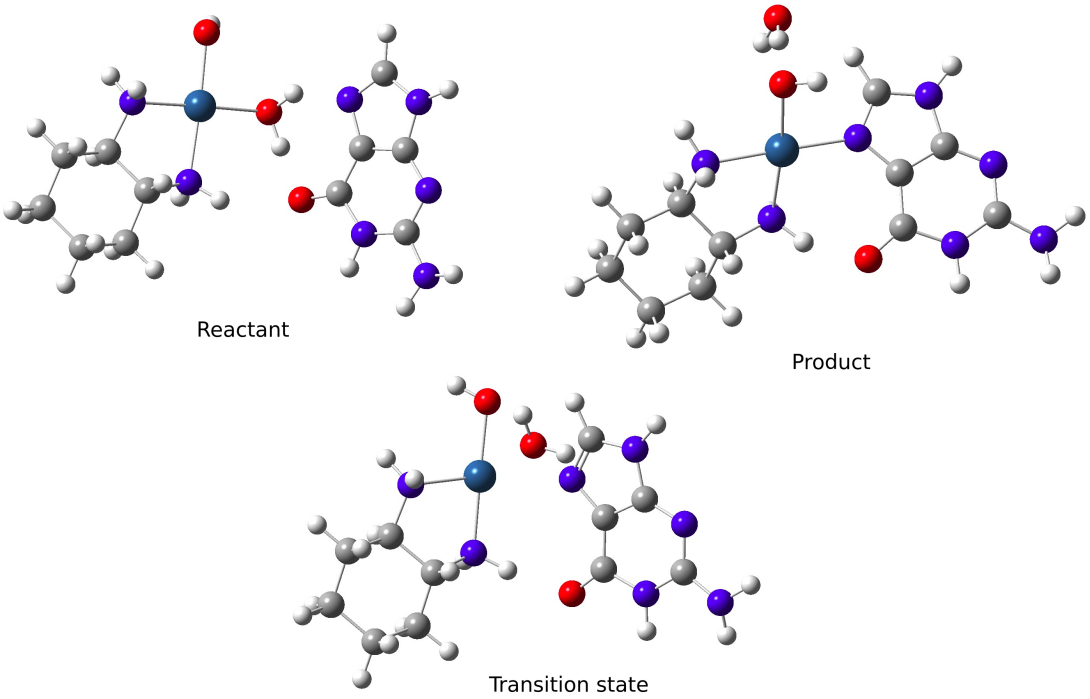

Figure .4.2: Reactant, transition state and product of reaction of Pt-Dach-OH with guanine.

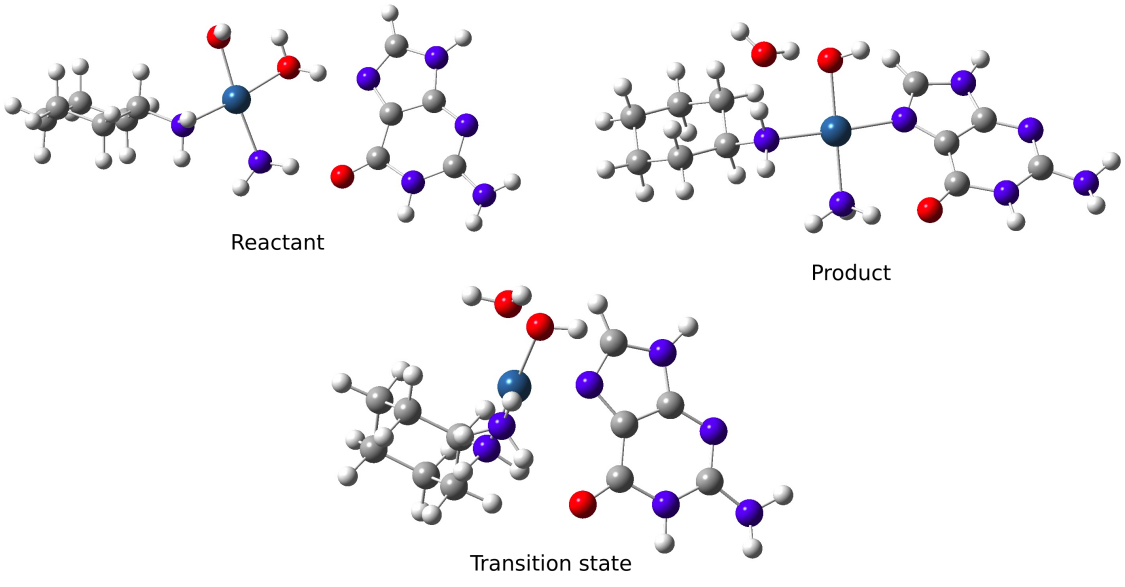

Figure .4.3: Reactant, transition state and product of reaction of JM118-OH with guanine.

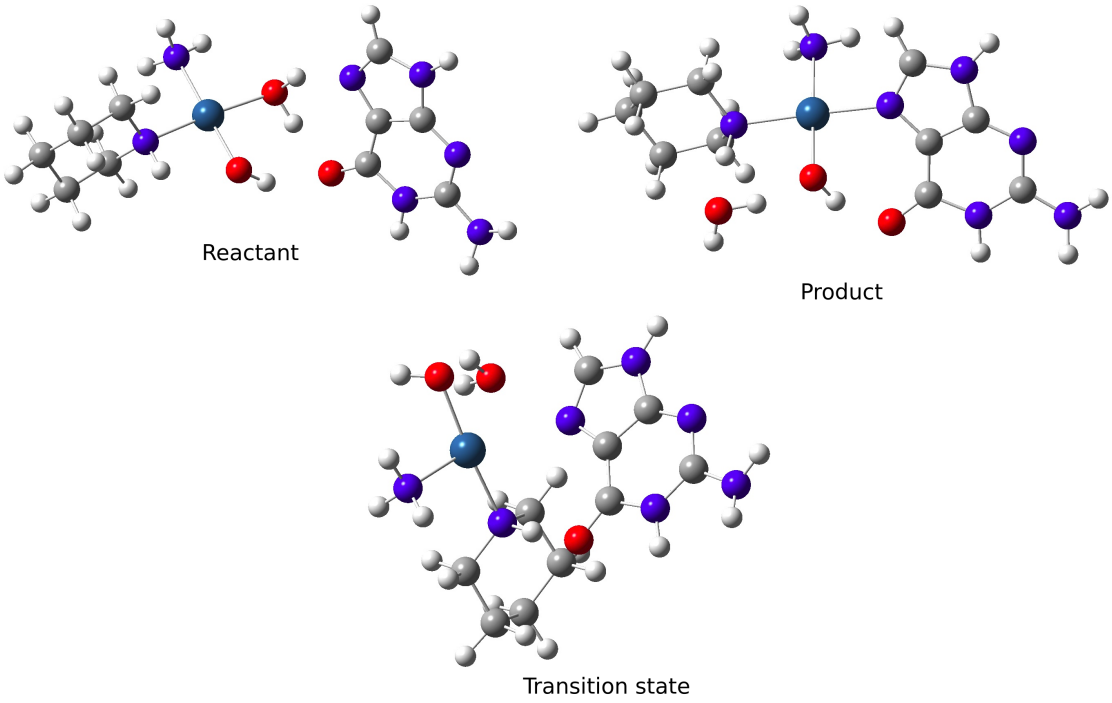

Figure .4.4: Reactant, transition state and product of reaction of Pt-Pip-OH with guanine.

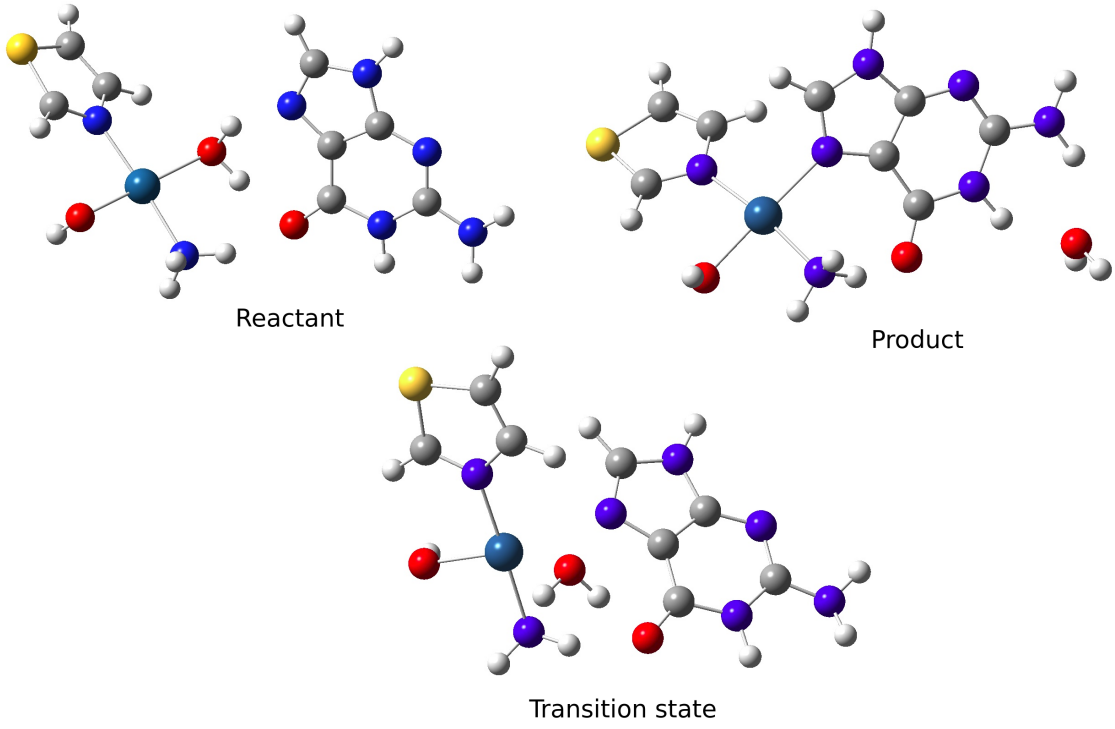

Figure .4.5: Reactant, transition state and product of reaction of Pt-Tz-OH with guanine.

.5 Basis set for Ru atom used in QM/MM calculations.

```
Ru   0
****
S    3   1.00
        7.93657000          -1.11966560
        5.98424500           1.44532930
        4.88222000          0.626165300
S    1   1.00
        1.14462400           1.00000000
S    1   1.00
       0.523017000           1.00000000
S    1   1.00
       0.117573000           1.00000000
S    1   1.00
       0.480500000E-01       1.00000000
S    1   1.00
       0.160000000E-01       1.00000000
S    1   1.00
       0.080000000E-01       1.00000000
P    2   1.00
        3.75460900          -4.72265650
        2.91657100           4.99090840
P    2   1.00
        1.04867500          0.728546700
       0.507320000          0.303904300
P    1   1.00
       0.267398000           1.00000000
P    1   1.00
       0.697480000E-01       1.00000000
P    1   1.00
       0.229270000E-01       1.00000000
P    1   1.00
       0.110000000E-01       1.00000000
D    4   1.00
```

```
        6.00991300          -0.327160000E-01
        2.10428000           0.265739200
       0.921500000           0.481239800
       0.388598000           0.409977800
D    1   1.00
       0.152836000           1.00000000
D    1   1.00
       0.510000000E-01       1.00000000
D    1   1.00
       0.250000000E-01       1.00000000
F   1   1.00
     1.29009561    1.00
```

.6 Pseudopotentials on Ru atom used in QM/MM calculations.

```
Ru   0
RU-ECP    4    28
G POTENTIAL
 1
2            1.00000000          0.00000000
S-G POTENTIAL
 2
2           11.10526900        209.82297100
2            5.41474500         30.65472600
P-G POTENTIAL
 2
2            9.77127100        146.33618200
2            5.07399100         24.12787700
D-G POTENTIAL
 2
2            7.67142300         67.51589700
2            4.13656500          9.87010400
F-G POTENTIAL
 2
```

2	11.36000000	−28.34061600
2	5.68000000	−4.94462900

.7 Stationary points of the reaction between the Ru(II) complex and the second guanine

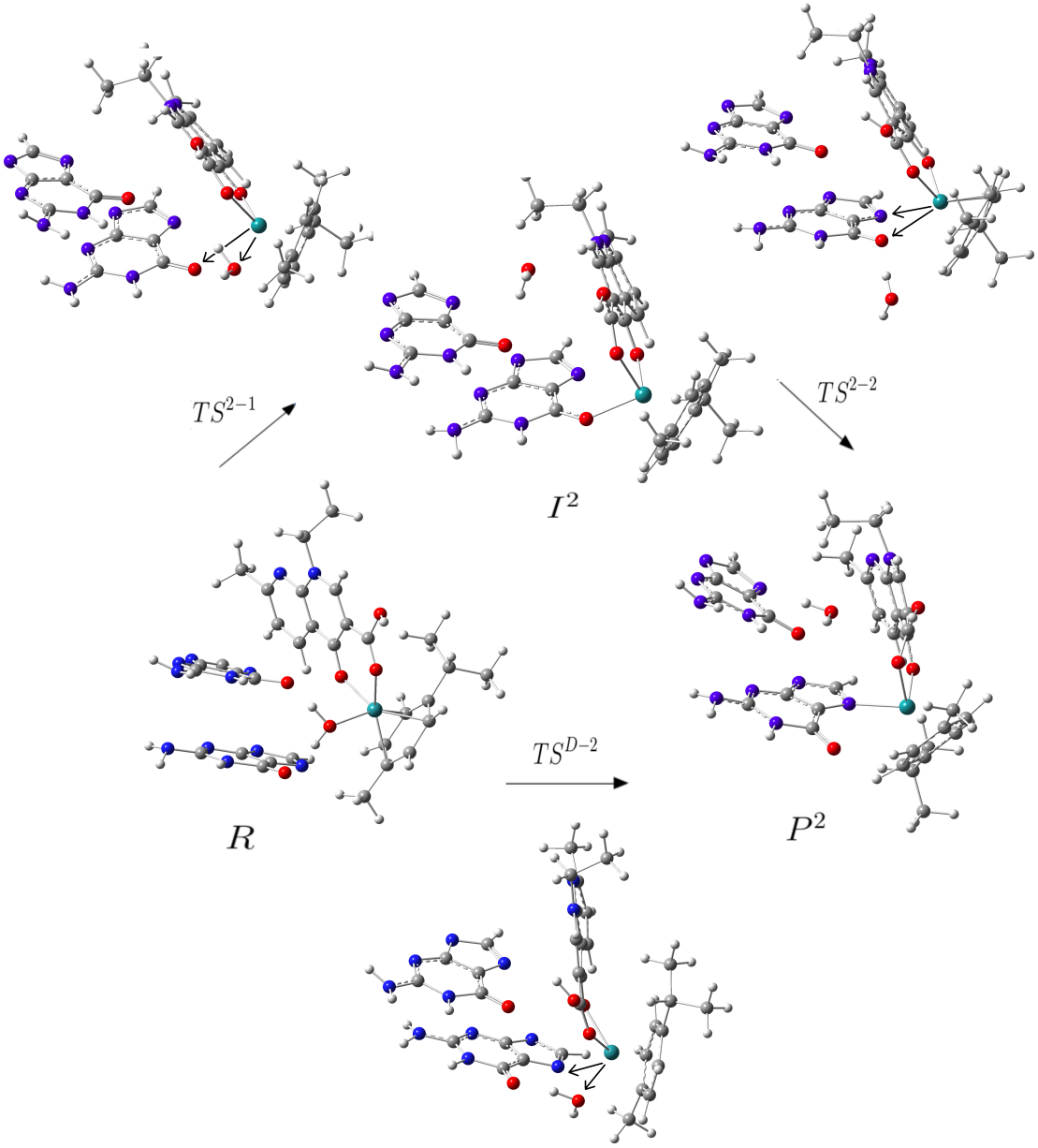

Figure .7.6: ONIOM optimized stationary points of the reaction between the Ru(II) complex and the second guanine. The black arrows correspond to the antisymmetric stretching movements.

.8 Stationary points of the reaction between the Ru(II) complex and DNA with opposite orientation of nalidixic acid

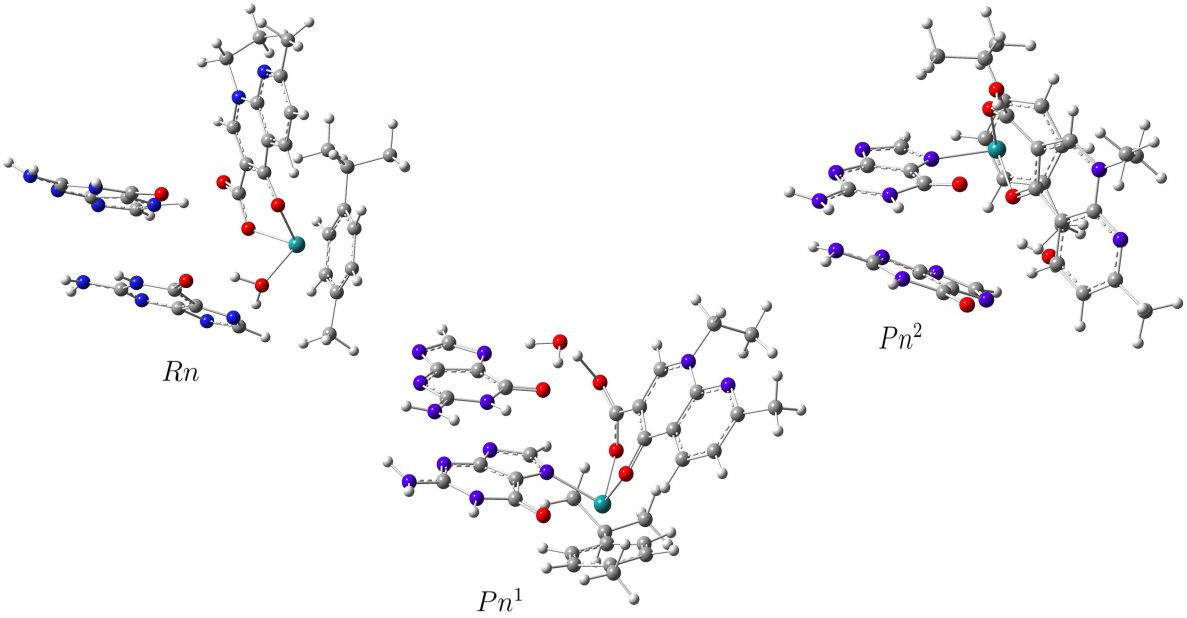

Figure .8.7: ONIOM optimized stationary points of chosen complexes with opposite orientation of nalidixic acid in the reaction of the Ru(II) complex with DNA.